

Original citation: J.X. Lu, P. Shen, Y. Zhang, H. Zheng, Y. Sun, C.S. Poon, Early-age and microstructural properties of glass powder blended cement paste: Improvement by seawater, *Cement and Concrete Composites* 122 (2021) 104165. <https://doi.org/10.1016/j.cemconcomp.2021.104165>

Early-age and microstructural properties of glass powder blended cement paste: Improvement by seawater

Jian-Xin Lu, Peiliang Shen, Yangyang Zhang, Haibing Zheng, Yanjie Sun, Chi Sun Poon*

Department of Civil and Environmental Engineering,
The Hong Kong Polytechnic University, Hung Hom, Kowloon, Hong Kong, China

*Corresponding author: jianxin.lu@polyu.edu.hk ; cecspon@polyu.edu.hk

Abstract: The incorporation of conventional supplementary cementitious materials (e.g. fly ash) in concrete generally induces a longer setting time and inferior early-age strength. This study aims to evaluate the effectiveness of using seawater (SW) as mixing water in improving the early-age properties of cement pastes/mortars prepared with waste glass powder (WGP) which has a low reactivity. By means of measurements of the rheological behaviors, macro/micro mechanical properties, hydration kinetics of the WGP blended cement with SW and other microstructural analytical techniques, the early-age performances were investigated. The results showed that the incorporation of WGP increased the yield stress and plastic viscosity of the cement paste due to its fine particle size, negative surface charge and hydrolysis effect. The use of SW further changed the rheological properties by accelerating the hydration of cement. The dissolved ions from the WGP and the presence of SW in the cement paste were beneficial to shortening the prolonged setting time induced by the replacement of cement by the WGP. The combined use of SW was effective in overcoming the inferior early-age strength caused by the dilution effect of WGP inclusion at the very early age. The enhanced precipitation of hydration products, increased degree of hydration, refined pore structure were responsible for the increase of the early-age strength of the WGP blended cement prepared with SW.

Keywords: Seawater; Glass powder; Rheology; Degree of hydration; Micromechanical property

1 Introduction

1.1 Research background

The conventional supplementary cementitious materials (SCMs), such as fly ash (FA) and ground granulated blast-furnace slag (GGBS), have been widely applied in the cement and concrete industry to reduce CO₂ emissions [1] and improve the durability of concrete [2]. However, there are shortages of the supply of these SCMs in some areas. It is becoming increasingly essential to explore alternative sources to meet the increasing demand of SCMs.

In Hong Kong, due to the lack of locally sourced conventional SCMs, waste glass powder (WGP) grinded from the post-consumed glass beverage bottles has recently been considered as an alternative SCM [3, 4]. As indicated by government statistics [5, 6], the average generation rate of waste glass was about 300 tonnes per day. However, the average recycling rate of waste glass was below 10% because of the lack of a local glass manufacturer. Thus, most waste glass is disposed of at landfills. So far, the major recycling channel of waste glass is using waste glass cullet to replace fine aggregates in the production of concrete paving blocks [6]. However, the amount that can be reused is limited. Thus, to reuse WGP as a replacement of cement in concrete/mortars may be another potential approach to broaden the recycling channel for waste glass.

The utilization of WGP as a supplementary cementitious material in concrete/mortars has attracted lots of research interests thanks to its pozzolanic activity [7-10]. The benefits of using WGP includes: 1) the reuse of WGP can reduce the disposal of waste glass and turn them into value-added resource; 2) the replacement of cement by WGP can reduce the cement consumption and CO₂ emission; 3) the incorporation of WGP could improve the long-term mechanical properties and durability of concrete/mortars [11-13]. However, similar to FA, WGP was found to have a low reactivity, which would prolong the setting time [14] and reduce the early strength of the blended cement significantly [3, 11]. The poor early age properties would limit its wider and high-volume applications. Therefore, it is necessary to improve the early age properties of WGP blended cement. Mechanical grinding is the most common method to increase the reactivity of WGP. The finer the particle size of WGP, the higher reactivity it has [3, 15]. Combining mechanical and thermal treatment methods was also effective in activating the pozzolanic activity of WGP in cement mortars [16]. A recent study suggested that immersing WGP in water for a certain time before contacting with cement and aggregates would increase the early strength of WGP containing concrete [17]. The formation of more

hydration products due to the partial hydrolysis of the WGP into Na and Ca ions in the water was responsible for the increased strength [17]. In order to improve the early age properties of mortars prepared with WGP, other more reactive materials, such as nano-silica [18] or silica fume [19], were jointly incorporated into the matrix to complement the low strength induced by the WGP. However, these approaches, to some extent, need to consume more energy/time or require the addition of high cost additives to counteract the inferior reactivity of WGP.

In recent years, attempts have been made to use seawater (SW) as mixing water in cement concrete/mortars with a view to meeting the demands of remote coastal construction and addressing the shortage of freshwater (FW) [20-22]. However, the major durability concern associated with the use of seawater in conventional reinforced concrete is the corrosion of steel bars [23]. Thanks to the availability of corrosion-resistant fiber reinforced polymer (FRP) bars, the SW and sea-sand have been successfully utilized for the production of reinforced concrete [24-27]. The seawater and sea-sand reinforced composites were reported to have comparable quasi-static mechanical properties and blast resistance in comparison with conventional concrete composites made with FW [26]. Also, the use of SW did not have detrimental impacts on the mechanical properties and bond behavior of FRP-bars [25]. For the application of seawater sea-sand concrete and FRP bars in shear walls, negligible effects were found on the short-term seismic performance as compared to the conventional reinforced concrete [27]. Based on experimental results and design-oriented model, the FRP confined concrete was regarded as a promising solution for offshore and marine construction due to the excellent corrosion resistance of FRP [28]. These encouraging results provide a potential to apply the SW as mixing water in cement-based materials. From the perspective of material performance, mixing with SW into the Portland cement concrete/mortars will inevitably influence their early age and later age properties due to the presence of dissolved salts in the SW. Although the findings on the effects of SW on the long-term age performance of concrete were contradictory [20, 23], however, most investigations agreed that the SW addition could reduce the setting time and accelerate the strength of cement-based materials at the early age [23, 29, 30]. On the basis of these characteristics, it is of strong interests to employ SW in the glass-based cementitious materials with a view to partly counteracting the inferior early-age properties caused by the inclusion of WGP with a low reactivity.

1.2 Research significance

For the concrete prepared with a large volume of low reactivity SCMs, prolonged setting time and low early strength will reduce production efficiency and increase cost. In this study, attempts were made to explore the feasibility of using SW as mixing water for improving the early age properties of cement paste or mortar blended with 20% WGP as a replacement of cement. The intended application of the proposed materials is non-structural aesthetic glass-based architectural cement mortars produced with the calender extrusion method [4, 18, 31]. Thus, it is essential to improve and understand the early age properties of the proposed mixture. This non-structure cement-based product without steel bars also favors exploiting SW as a mixing water. Japanese Concrete Institute [32] has published a technical committee report in 2015 to investigate the possibility of seawater usage in concrete production, which pointed out that seawater can be used almost 100% as mixing water in plain concrete and concrete with stainless steel. As the report suggested, mixing concrete with seawater had little effect on the long-term strength of the concrete and was able to improve other properties, such as reduced water permeability and reduced drying shrinkage.

Another purpose of this study was trying to reduce the consumption of FW in construction projects. According to The United Nations World Water Development Report 2019 [33], more than 2 billion people (nearly one-third of the world population) are experiencing severe water scarcity. As shown in Fig. 1, many countries, including China, India, and in particular the North Africa and the Middle East, are facing water stress of higher than 25% (the minimum threshold of water stress). To cope with the increasingly water scarce, saving water in the construction area is imperative.

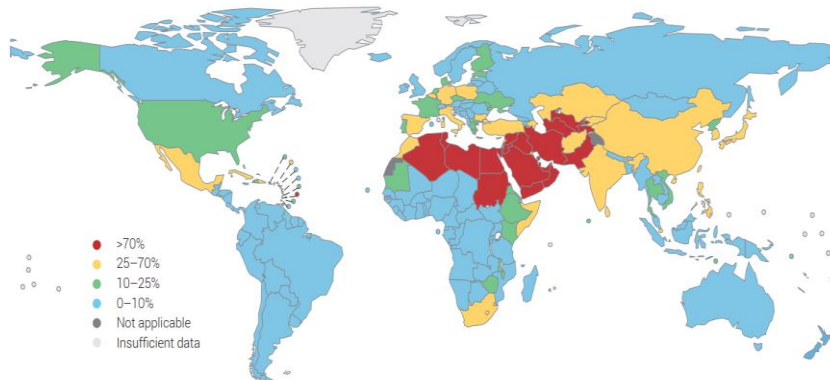


Fig. 1. Level of physical water stress by country (%) [33].

This work focuses on evaluating the effect of SW on the cement paste/mortar prepared with low reactivity WGP. The glass material and SW will be utilized collectively for partially

replacing binder, aggregates and completely the mixing water. A comprehensive experimental programme including rheological behaviors, macro and micro-scale strength at very early age, early hydration was conducted. In addition, the mineralogy analysis, thermal stability and pore structure of the system containing WGP were also investigated.

2 Materials and methods

2.1 Materials

2.1.1 Cement and WGP

A Type I white ordinary Portland cement (WPC) was employed as the main cementitious material since the glass-based architectural products require good aesthetic appearance [4, 31]. The WPC compliant with ASTM C150 [34] was sourced from Green Island Cement Company Limited in Hong Kong. WGP was produced by grinding glass cullet, which was crushed from waste glass beverage containers (mixed color) [35]. A laboratory ball mill (a cylindrical barrel with internal diameter of 260 mm and length of 330 mm) was used for grinding the glass cullet. The rotation speed of the ball mill was 60 r/min and the mass ratio of steel balls to glass cullet was 6:1. The milling time was set to 4 hours. It should be noted that the WGP was nearly white in color although the glass bottles were mixed colored. The chemical compositions of the WPC and the WGP were characterized by X-ray fluorescence using a Rigaku Supermini200 spectrometer. The results are listed in Table 1. The rich SiO₂, CaO and Na₂O in the WGP was the typical characteristic of soda-lime-silica glass.

Table 1. Chemical compositions and mineral phases of WPC and WGP (wt. %).

Compositions	WPC	WGP
SiO ₂	21.2	69.0
Al ₂ O ₃	5.10	2.62
CaO	67.9	10.5
MgO	1.21	1.35
K ₂ O	0.12	0.79
P ₂ O ₅	0.12	0.12
Fe ₂ O ₃	0.21	1.42
Na ₂ O	-	13.5
SO ₃	4.12	0.13
Mineral phases (determined by Q-XRD)		
C ₃ S	50.52	
C ₂ S	40.88	
C ₃ A	6.89	Amorphous
Gypsum	1.60	

Free-CaO	0.11	
Physical properties		
Density (g/cm ³)	3.03	2.37
Average particle size (μm)	17.7	20.4

2.1.2 Physical and morphological characteristics of WPC and WGP

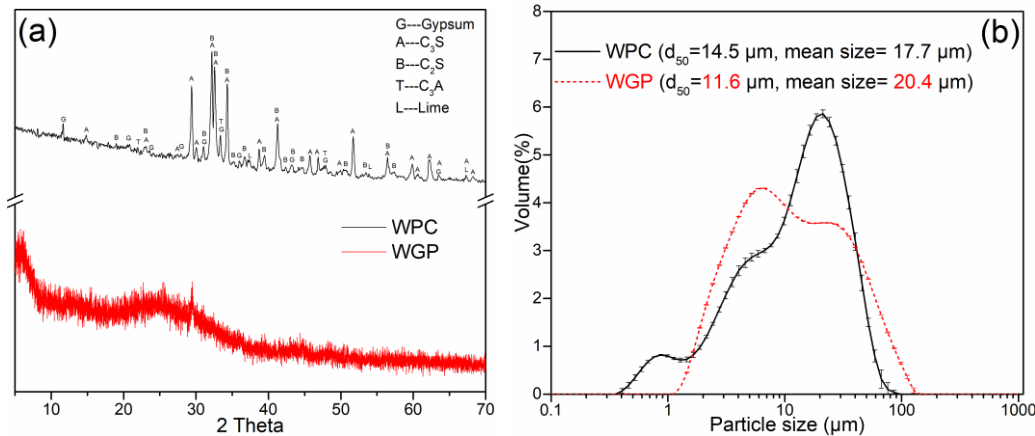


Fig. 2. XRD patterns (a) and particle size distributions (b) of WPC and WGP.

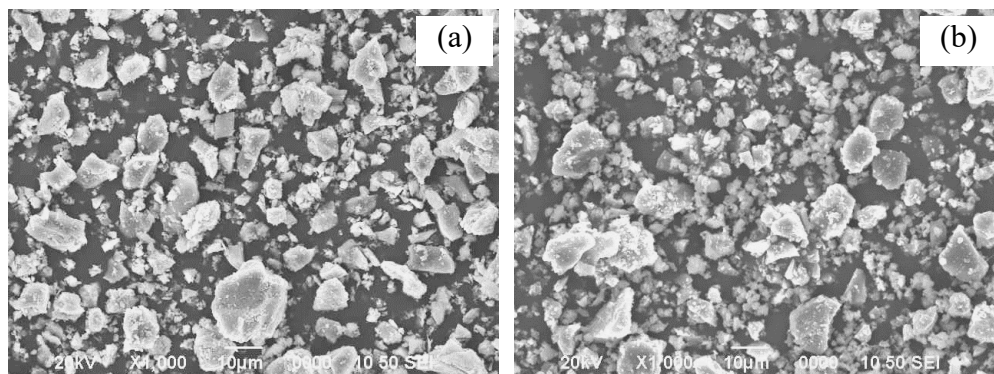


Fig. 3. Morphologies of WPC (a) and WGP (b).

The mineral phases in the WPC were determined by Rietveld refinement of quantitative X-ray diffraction (Q-XRD) analysis (Fig. 2a). The contents of tricalcium silicate (C₃S), dicalcium silicate (C₂S) and tricalcium aluminate (C₃A) were 50.52%, 40.88%, 6.89%, respectively. The lack of ferrous phase (C₄AF) in the cement due to the extremely small amount of Fe (Table 1) may result in a relatively high C₂S content. No crystalline peaks in the WGP indicate the amorphous structure of glass. The particle size distributions (PSD) of WPC and WGP were measured by a laser diffraction particle size analyzer (Malvern Mastersizer 3000E) in Hydro EV mode. The dispersive solutions for WPC and WGP were ethanol and water, respectively, with a stirrer speed of 2,330 rpm and ultrasonication level of 30%. The results are depicted in Fig. 2b, which shows that the d₅₀ value of WGP was smaller than that of WPC, while the average particle size of WGP was coarser than that of WPC. Scanning electron microscopy (JEOL Model, JSM-6490) was employed to observe the morphologies of WPC and WGP (Fig.

3). The images show similar appearance between the cement and the WGP. Both of them had a vitreous structure, but the WGP seemed to have more fine particles, which was in agreement with the PSD results.

2.1.3 Glass aggregates and SW

The fine glass aggregates were obtained by crushing post-consumer beverage bottles, sourced from a recycling facility in Hong Kong. The glass aggregates were cleaned by fresh water to remove impurities (e.g. papers and plastics). Then, the aggregates were transferred to an oven for drying at 105 °C for 24 hrs. The density and water absorption of the glass aggregates were 2.48 g/cm³ and 0.13%, respectively. The gradation of the glass aggregates shown in Table 2 was within the limits of BS 822 standard. It should be noted that the incorporation of 20% WGP in this study was effective in suppressing the ASR expansion of 100% glass aggregates, which has been confirmed in our previous studies [4, 31].

The natural SW was collected from the Victoria Harbor in Hong Kong. An inductively coupled plasma/optical emission spectrometry (ICP-OES, FMX 36, SPETROBLUE) was used to identify the quantities of cations in the SW. An ion chromatography (Thermo Scientific Dionex Aquion) was used to determine the anions in the SW. Prior to both tests, the SW was diluted for 500 times. The components of SW are shown in Table 3, which indicate that the predominant ions in the SW were sodium and chloride, and certain amounts of magnesium and SO₄²⁻ were also detected.

Table 2. Gradation of glass aggregates.

BS sieve size (mm)	10	5	2.36	1.18	0.6	0.3	0.15
Passing (%)	100	99.94	84.64	57.56	27.74	8.81	1.62

Table 3. Elemental components of natural SW (mg/L).

Na	K	Ca	Mg	Al	Cl ⁻	SO ₄ ²⁻
10140	960	426	1306	170	18822	2465

2.2 Mix proportions

Cement paste was adopted for the evaluation of early age performance in order to provide a clearer understanding of the effect of SW on the rheology and hydration of different binders.

The early strength tests were performed on cement mortars prepared using 100% glass as aggregates. Four mixtures were designed with and without 20% replacement of WGP by mass. Natural SW was used to mix with the pure WPC and WGP-based binder at a water-to-binder (*w/b*) ratio of 0.4 as shown in Table 4. For the macro-mechanical properties, cement mortars were used with an aggregate-to-binder ratio of 2.0. The pastes used were the same as that in Table 4, and the glass cullet was employed as 100% fine aggregates with a view to promote the recycling rate of waste glass. Another purpose was to enhance the aesthetic appearance of architectural products as indicated in a previous study [4]. In order to improve the workability of the mortars, a small dosage of superplasticizer ADVA-109 (W.R. Grace) was added based on the binder mass (0.6%).

The codified mix ID comprised two alphabet character parts. The “CON” refers to the mixture prepared with pure WPC as binder. The “WGP” denotes the binder containing 20% WGP as a replacement of cement. The “FW” and “SW” mean the mixing water was freshwater and seawater, respectively.

Table 4. Mix proportions of cement pastes mixing with FW and SW.

Mix	WPC	WGP	Water	<i>w/b</i>
CON-FW	1	0	Freshwater	0.4
CON-SW	1	0	Seawater	
WGP-FW	0.8	0.2	Freshwater	
WGP-SW	0.8	0.2	Seawater	

2.3 Methods

2.3.1 Rheological properties

The rheological behavior tests of the cement pastes were conducted at 20 °C using a rheometer (RST Brookfield 3000) equipped with a vane spindle (VT-60-30). The measurement was carried out at 4 mins (including 2 mins’ mixing) after the dry materials came into contact with water. The shear rate was programmed as a function of time and is shown in Fig. 4a. Five cycles were performed in each test. At each cycle, the shear rate was increased from 0 to 100 s⁻¹ in 50 s and then the maximum rate was kept constant for 20 s. Afterwards, the shear rate was decreased from 100 s⁻¹ to 0 in 50 s. A 10 mins rest (0 s⁻¹) was set in the interval of the cycles for paste hardening. The protocol for measuring each sample took over 50 mins. The shear stress against shear rate was recorded for calculating the rheological characteristics (yield stress and plastic viscosity). Fig. 4b shows the typical shear stress-shear rate curves of

the pure WPC pastes, including the ascending and descending curves. Usually, in the descending part of the hysteresis loop, the linear relationship between the shear stress (τ) and the shear rate ($\dot{\gamma}$) of the cement paste followed the Bingham model as expressed by Eq. (1) [36]. The rheological parameters can be obtained by the following equation.

$$\tau = \tau_0 + \eta \dot{\gamma} \quad (1)$$

Where τ_0 is yield stress (Pa), η is plastic viscosity (Pa·s).

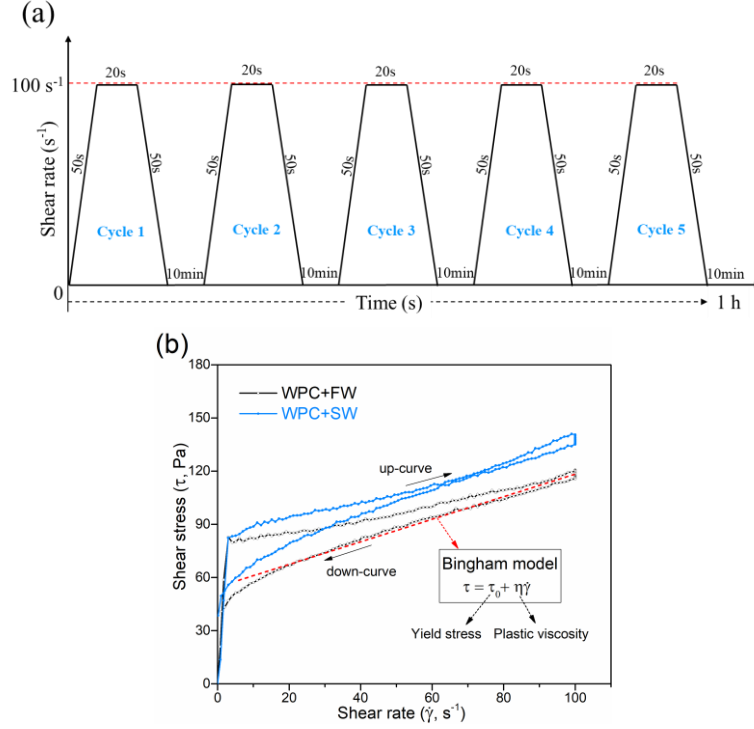


Fig. 4. Shear rate profile as a function of time (a), and the typical shear stress-shear rate curves of cement pastes prepared with FW and SW (b).

The workability characteristics of the fresh cement paste were evaluated by a flow table test following EN 1015-3/A2 [37]. A copper mini-cone with size of 36×60×60 mm was used to load the fresh paste according to GB/T 8077 [38]. The paste was filled into the cone when the dry materials were mixed with water for 2 mins. After lifting the cone vertically at 3.5 mins, the initial flow values of the paste spreading out on the disc were measured at three directions. Afterwards, by jolting the flow table for 15 times at a constant frequency, three spread diameters (d_1 , d_2 and d_3 , mm) of the paste were further recorded as vibrated flow. To better understand the deformability of the mixture, relative flow area (Γ_R) was calculated analogously to the study of Domone and Chai [39].

$$\Gamma_R = \left(\frac{d_1 + d_2 + d_3}{3d_0} \right)^2 - 1 \quad (2)$$

Where Γ_R is relative flow area, d_0 is the base diameter of the cone (60 mm in this case).

The setting time is commonly used to determine the stiffening characteristic of the cement paste. To study the effect of SW addition on the early age hardening behavior of the pastes with and without WGP, a Vicat apparatus was employed to determine the initial and final setting times of all the mixtures according to BS EN 196-3 [40]. The proportions of mixture are shown in Table 4. Two measurements were carried out for each mixture.

2.3.2 Early mechanical properties

Mortar samples using 100% glass as aggregates were prepared for compressive strength test. The binders prepared in accordance to Table 4 were mixed with the aggregates firstly and then FW/SW was poured into the mixer to produce the homogenous mortars. After mixing, the fresh mortars were cast into steel cube molds with size of 50×50×50 mm. 15 s of mechanical vibration was allowed on a laboratory vibration table for compacting the fresh mixtures. A plastic sheet was used to cover the surface of molds to avoid moisture evaporation. After the mortars were cured in the molds for 24 hrs, the samples were demolded and the 1-day compressive strength was tested at a loading rate of 0.6 MPa/min in accordance with ASTM C109 [41]. Other samples were placed into a water tank for further curing at a temperature of 25 °C. After another 2 days curing, the 3-day compressive strength of the mortars were measured. Three samples were tested to obtain an average value at each age.

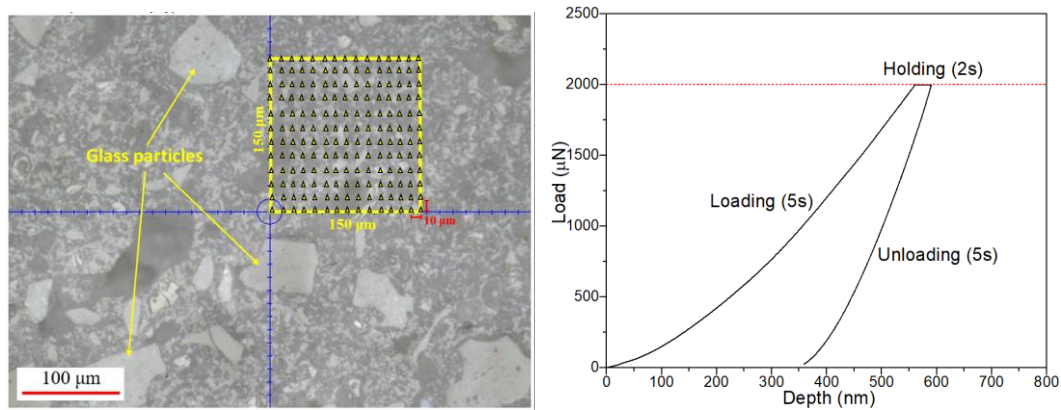


Fig. 5. (a) Nanoindentation protocol of the cement paste, (b) Typical load–depth curve for a nanoindentation test.

The nanoindentation technique was regarded as an effective approach in determining the micro/nano mechanical properties of cement-based materials [42]. In this study, a Bruker’s Hysitron TI Premier nanoindenter was used to measure the qualitative and quantitative micro-scale mechanical characteristics of the cement pastes. The equipment had a displacement range from 0.2 nm to 5 μm and a load range from 75 nN to 10 mN. A diamond tip with Berkovich

triangular pyramidal was equipped for the nanoindentation measurement. A square indentation grid of 225 points (15×15) was set to implement the indentation as shown in Fig. 5a. An interval spacing of $10 \mu\text{m}$ between grids was used to avoid interference of each indentation. The indentation program was a trapezoid loading as presented in Fig. 5b. The maximum force of $2000 \mu\text{N}$ was reached at a rate of $400 \mu\text{N/s}$ and then was maintained for 2 s, followed by unloading within 5 s. Based on the displacement depth and the load, elastic modulus and hardness of the indented point can be calculated [43, 44].

With regards to the preparation of samples for the nanoindentation test, fractured cement pastes whose hydration have been stopped were embedded in an epoxy resin (Epo Thin 2) under vacuum condition. The impregnation of epoxy resin was to solidify the fractured and uneven samples in a mould. The epoxy resin was completely hardened after 24 hrs, thus it provided support for the samples during the grinding and polishing processes. Then, the hardened samples were gently ground in a Buehler polisher (Auto Met 300) by grit 320 paper until removing the epoxy resin covering on the surface of the paste. Afterwards, grits 600 and 1200 papers were separately used to grind the samples for 3 mins. In order to achieve a smooth surface for nanoindentation tests, the samples were further polished by grits $9 \mu\text{m}$, $3 \mu\text{m}$, $0.05 \mu\text{m}$ diamond/alumina papers for 30 mins accompanying with monocrystalline diamond suspension (MetaDi), respectively. After finishing the above steps, the samples were immersed in anhydrous ethanol for ultrasonic cleaning for 5 mins to remove the residual polishing particles on the sample surface. Before the nanoindentation tests were performed, the samples were dried in a vacuum oven at $60 \text{ }^\circ\text{C}$ for 12 hrs. It should be noted that, after polishing process, the surface roughness of the samples pre-tested by in-situ Scanning Probe Microscopy installed with the nanoindenter was refined within 150 nm to minimize its effect on the results.

2.3.3 Isothermal calorimetry

The heat of hydration was monitored to explore the influence of SW on the hydration of the binders with and without WGP incorporation. The paste proportions were prepared in conformity with the mix proportions in Table 4. 60 g of dry powder was thoroughly mixed with 24 g of FW/SW within 2 mins in an insulated container. Afterwards, the container was transferred into the isothermal calorimeter (Calmetrix I-CAL) with four channels. The calorimeter was controlled at a constant temperature of $20 \text{ }^\circ\text{C}$. After recording the heat flow of hydration up to 72 hrs, the data were exported and analyzed.

2.3.4 Zeta potential and Na concentration

The zeta potentials of C₃S, C₃A, WPC and WGP in water were determined (Malvern, Zetasizer Nano Series) to assess the surface charges of the main clinker phases, cement and glass particles. The C₃S and C₃A were obtained commercially from mainland China, and the purities of C₃S and C₃A were 94 wt.% and 90 wt.% determined by Q-XRD analysis. The ratio of solid samples to deionized water used was 1:100 to ensure excess water for hydration and dissolution. After 2-min mixing, the supernatants were separated from the solids by using a centrifuge at 4,000 rpm for 2 mins (Dynamica, Velocity 18R). Approximate 1 mL of suspension was injected into a folder capillary cell for measurement. The average zeta potential data was obtained by 3 measurements.

The ions dissolved from the WGP in FW and SW were measured by a Cole-Parmer single-channel flame photometer (EW-02655). The ratio of WGP to FW/SW was 1:2 based on the proportion in Table 4. After mixing the solutions for 5 mins, 10 mins, 20 mins, 30 mins, 1 h, 3 hrs, 6 hrs, the supernatants were obtained using the same procedure as the zeta potential measurement, and then was filtered through a 0.45 μm membrane filter. The pH of the filtrate was measured by a pH meter and Na concentration of the diluted filtrate was tested by a flame photometer. The values were reported based on the average of 3 measurements.

2.3.5 Microstructure tests

The samples for the microstructure tests were cement pastes prepared according to Table 4. After curing for 1 day and 3 days, the pastes were broken up into fragments and soaked into anhydrous ethanol to stop the cement hydration. After one week of immersion, the small pieces of pastes were transferred to a vacuum oven at a constant temperature of 60 °C for one week to remove the residual ethanol. The fractured samples were used for porosity testing. For the mineralogy and thermal stability analyses, the above fragments were ground into powdered samples (less than 63 μm) for measurements.

X-ray diffraction (XRD, Rigaku SmartLab-Advance) was used to identify the crystalline phases of the cement pastes prepared with FW and SW. The XRD was equipped with 9 kW rotating anode X-ray source ($\lambda \sim 1.54\text{\AA}$) and a high-quality two-dimensional semiconductor detector (HyPix-3000). Parallel beam mode was applied to measure the powder samples with a 0.01° step size. The scan range (2θ) from 5° to 70° was selected in the measurement. The X-ray operation was performed at 45 kV and 200 mA with CuK α radiation. For quantifying the

crystalline phases in the cement paste, the powdered samples were mixed with 20 wt% of Al₂O₃ as internal standard and Rietveld refinement was performed by using Topas 4.2 software.

Thermogravimetric (TG, Rigaku Thermo Plus EVO2) analysis was conducted on powdered samples to quantify the phase decomposition at different temperature ranges. The test method was performed in accordance to ASTM E1131 [45]. Around 10 mg powder placed in a corundum crucible was used for testing. The samples were heated from 30 to 1000 °C at a rate of 10 °C/min under argon gas environment. The chemically bound water (H₂O_{bound}) within the C-S-H gel and free portlandite (CH) could be estimated based on the TG measurement to assess the degree of reaction of the binders [46]. The bound water loss due to the carbonation of CH was also taken into account. Hence, the value of chemically bound water was calculated by the sum of the dehydration, dehydroxylation and the decarbonation losses. The estimation of H₂O_{bound} normalized to the original mass can be determined by using Eq. (3) based on [47]. Deboucha et al. [48] pointed out that the ultimate bound water (H₂O_{bound}) of a pure cement paste could be estimated after a few months, and the pozzolanic materials-containing cement achieved the highest degree of hydration after one year. Thus, in this study, four-year-old cement pastes with the same mix proportions were measured by TG-DTG to obtain the H₂O_{bound} content and it was regarded as the ultimate hydration degree. Therefore, the relative degree of hydration (DoH) of cement pastes in this study was defined as the ratio of the H₂O_{bound} at the early age to the corresponding H₂O_{bound} of the four years paste according to Eq. (4).

$$H_2O_{bound}(\%) = (M_{50^{\circ}C} - M_{CH}) + \frac{18}{44}L_{CC} \quad (3)$$

Where M_{50°C} and M_{CH} are the mass losses at 50 °C and 450 °C, respectively. The first part (M_{50°C} - M_{CH}) means the bound water between 50 °C and 450 °C. The selection of 50 °C rather than 105 °C is to avoid the water removal from the AFt, AFm and C-S-H. The second part is the bound water equivalent to the decarbonation loss. It is assumed that the calcium carbonate was formed by carbon dioxide reacting with CH. The temperature regions were selected based on the DTG curves.

$$DoH(\%) = \frac{H_2O_{bound}(EA)}{H_2O_{bound}(4Y)} \quad (4)$$

Where DoH is the degree of hydration of the cement pastes, H₂O_{bound} (EA) is the DoH of the early age cement pastes and H₂O_{bound} (4Y) is the DoH of the four years old cement paste.

A mercury intrusion porosimeter (MIP) was employed to analyze the pore structure of the cement pastes according to ASTM D4404-10 [49]. The mercury porosimeter used (Micromeritics AutoPore IV 9500) covered the pore diameter range from approximately 360

μm down to 5 nm with a maximum mercury intrusion pressure of 207 MPa. Thus, this technique focuses on detecting the categories of air voids and capillary pores (not include the nanometer-sized gel pores) [46]. The sample preparation method for MIP test had been described above. The contact angle of the mercury on the sample surface was taken as 140° in the intrusion experiment. The method assumed that the pore shapes were cylindrical based on Washburn equation. In the MIP results, it should be noted that the ink-bottle effect would lead to an overestimation of small pores and an underestimation of large pores [46].

3 Results and discussion

3.1 Rheological behaviors

3.1.1 Yield stress and plastic viscosity

The rheological properties of the fresh WGP blended pastes prepared with FW and SW are displayed in Fig. 6. The yield stress almost linearly increased with the increase of cycle (i.e. time) due to the continuous formation of hydrates, regardless of using FW or SW. When the pure cement paste was mixed with SW, the dynamic yield stress was increased obviously at all cycles. The much higher yield stress was due to the acceleration of cement hydration (to be discussed in Section 3.3). The decreased free water in the system as a result of accelerated hydration would lead to higher cohesion and internal friction between the particles. Furthermore, larger quantities of colloidal hydration products in the SW paste required a higher shear force to break down the stiffened structure.

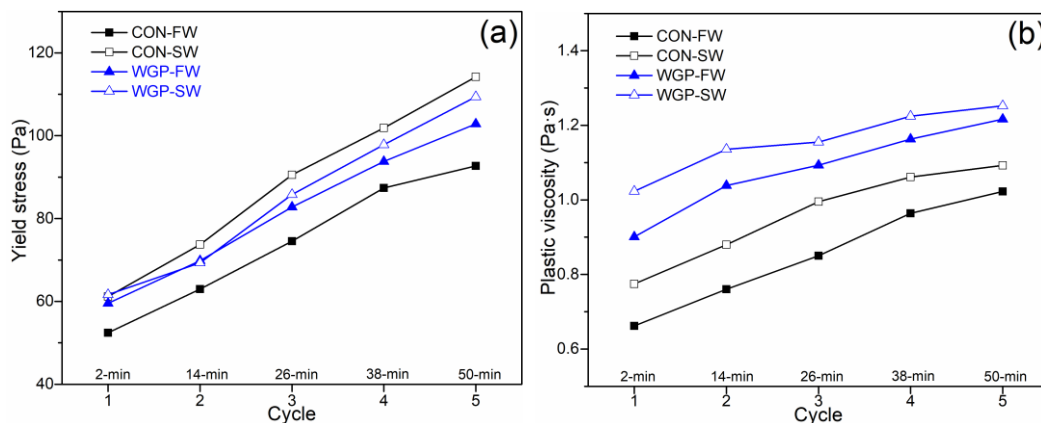


Fig. 6. Rheology of control and WGP pastes prepared with FW and SW: (a) Yield stress and (b) Plastic viscosity.

For hydrating with FW, when WGP was incorporated to replace part of the cement, it is found that the yield stress was higher than the pure cement paste at all cycles. This appears to be contradictory to the dilution effect of WGP incorporation since the reduced amount of cement would obviously produce less quantities of solid hydration products at this early age. The dissolution and physical properties of the WGP might play important roles in controlling the

rheological behaviors. When the WGP contacted with water, some ions, such as Na and Ca, would leach out from the WGP into water [50], which might accelerate the hydration of cement [51, 52]. However, the WGP was proven to be a lowly reactive material in the cement-based system [18, 53], especially at this very early stage. Hence, it is expected that the dissolution and pozzolanic reaction of WGP had little effects on the stiffening of cement paste within 1 hour. A previous study [14] also showed that the use of 20% WGP by mass as a substitution of cement enhanced the stiffening rate of cement mortars. Therefore, it is suggested that, in the WGP blended paste, the yield stress at this early age was primarily dependent on the physical properties of WGP, such as specific density and particle characteristics (particle size and shape, and surface charge). Table 1 shows that WGP has a lower density than that of cement, suggesting that the same mass replacement of cement by the WGP increased the volume of dry materials. Furthermore, as shown in Fig. 2, the d_{50} value of WGP was lower than that of cement. The finer particles had a higher specific surface that required more water for lubrication to achieve the same consistency. Also, worth noting is a slight increase in yield stress of WGP containing paste prepared with SW. However, it should be noticed that the increase of yield stress with the use of SW in the WGP incorporated paste was not as significant as that of the pure cement paste. The yield stress is controlled by the interaction of the particles in the fresh paste, and the uniform distribution of WGP particles in the paste would hinder the connection of the hydrates albeit the accelerating effect of SW.

Fig. 6b also illustrates the change of plastic viscosity with time in the WGP blended cement pastes prepared with FW and SW. It can be clearly noted that the using of SW increased the viscosity of the pure cement paste. Kondo et al. [54] suggested that the greater anion mobility of Cl^- promoted the dissolution of cement and formation of insoluble calcium hydroxide. Indeed, mixing single salts of the SW with alite was verified to speed up alite dissolution and precipitation of hydration products [55].

It is of interest to note that the incorporation of WGP significantly increased the plastic viscosity of the cement paste. The fineness, surface charge and the ion dissolution of the WGP were three most important factors affecting the viscosity: 1) as shown in Fig. 3, the WGP had more fine particles so that the replacement of cement by WGP could give rise to a more compact mixture, which led to an increase of viscosity; 2) the zeta potential results in Fig. 7 indicates that the WGP particles possessed negative surface charges while part of clinker phases such as C_3S had positive surface charges. Therefore, it is inferred that the inclusion of WGP would likely increase the attractive forces between the WGP and the clinker particles due to the electrostatic interaction, especially for C_3A with high positive charges; 3) another possibility would be that the immediate hydrolysis of WGP released dissolved ions in water

(to be discussed in Section 3.3) and resulted in an increased concentration of ions in liquid, which caused a higher plastic viscosity of the paste.

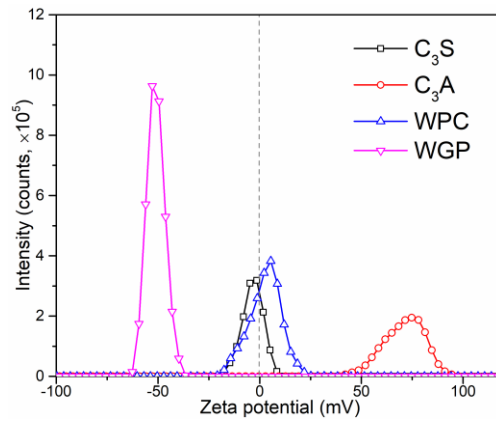


Fig. 7. Zeta potentials of C_3S , C_3A , cement and WGP in water (solid/deionized water = 1:100).

3.1.2 Workability

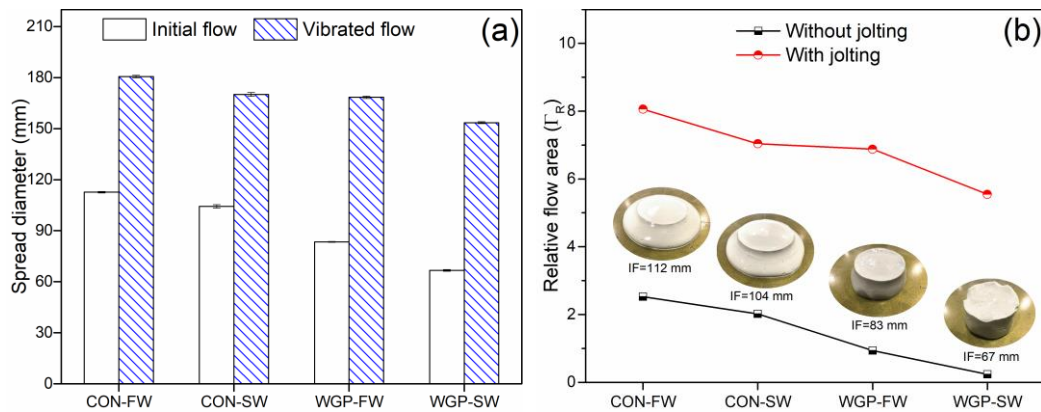


Fig. 8. Workability of control and WGP pastes mixed with FW and SW: (a) Flow spread and (b) Relative flow area (Γ_R).

The workability of cement paste incorporated with WGP and SW is presented in Fig. 8. Mixing SW with pure cement decreased the flow value as compared to the FW cement paste. However, the reduction was only marginal because the accelerated hydration was quite low within the first few minutes. When the WGP was used to replace cement, the workability of blended paste was largely reduced attributed to the increase of viscosity as shown in Fig. 6b. Since the viscosity was increased further by using SW, the flowability of the paste decreased regardless of jolting was used or not.

In order to demonstrate the flow characteristics and the deformability of the fresh pastes, the relative flow area (Γ_R) calculated is shown in Fig. 8b. The initial Γ_R was obtained by measuring the paste without subjecting to jolting, hence the deformation of paste was solely

resulted from its self-weight. A Γ_R of 0 means that no slump and deformation took place. The reduction in the Γ_R by mixing with SW suggested that the deformation of the paste was slowed down. It can be noted that the incorporation of WGP further reduced the Γ_R of the paste. This indicates that water in the blended paste was retained rather than acted as a lubricant among the particles. The WGP incorporated paste seemed to retain the shape of cone as shown in the images of initial flow (Fig. 8b). Combined use of WGP and SW lowered the Γ_R to a greater extent ($\Gamma_R = 0.236$). Visual inspection in Fig. 8b also indicated that the paste exhibited less deformation and maintained a good plasticity after demolding. As mentioned before, the flowability and the deformability of the paste may be dependent on the rheological properties, such as plastic viscosity. To validate this hypothesis, the relationship between the Γ_R and the plastic viscosity is depicted in Fig. 9. The Γ_R linearly decreased with the increase of viscosity. The good agreement validates that the flowability of the paste with and without jolting was associated with or even controlled by the fundamental rheological properties. In other word, the rheological properties would be possible to be estimated from the results of simple flow spread test. As the intended production method of the proposed mixtures in this study was calender extrusion, good shape stability and deformation capacity of the paste under an external force would be beneficial for producing the extruded products.

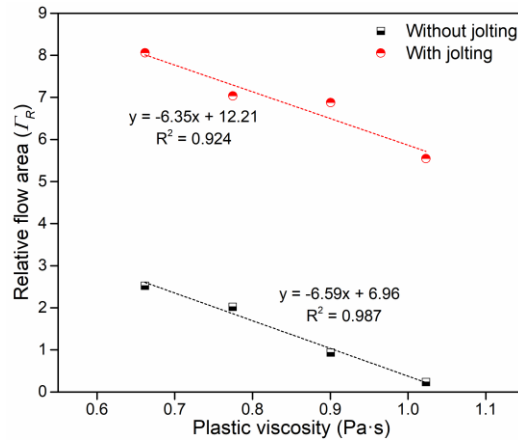


Fig. 9. Relationship between relative flow area (Γ_R) and plastic viscosity.

3.1.3 Setting time

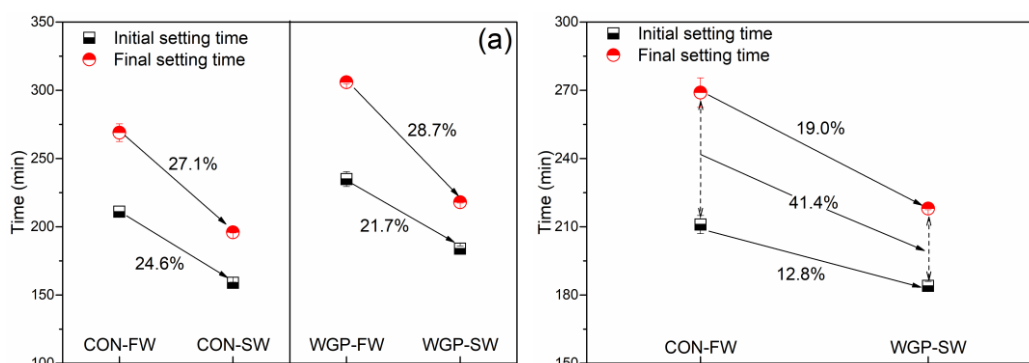


Fig. 10. Setting times of control and WGP pastes prepared with FW and SW.

Fig. 10 displays the initial and final setting times of the cement paste incorporated with WGP and SW. The replacement of FW by SW significantly shortened the setting times of the pure cement paste. Most researchers agreed that the chloride ions and other cations in SW could accelerate the dissolution of C_3S phase in cement [52, 54, 56]. Since cement setting occurred during the induction period, in which the nucleation and growth of hydration products began, and in this period, SW could promote the aggregation of the small floccules to accelerate setting and stiffening.

When WGP was incorporated into the cement, the setting times were delayed. This phenomenon can be interpreted in terms of three aspects [14, 18]: 1) dilution effect by replacement of cement; 2) non water absorbing nature of WGP increased the effective water-to-cement (w/c) ratio; 3) low reactivity of WGP. However, it is found that the use of SW as mixing water could significantly decrease the setting times. For the WGP blended cement prepared with SW, the initial and final setting times were decreased by 28.7% and 21.7%, respectively, as compared to those prepared with FW. Furthermore, the interval between the initial setting to final setting was shortened. This result indicates that using SW was effective in shortening the setting times of the WGP incorporated pastes. Fig. 10b presents a comparison of the setting of the control paste prepared with FW and the WGP blended paste prepared with SW. It is worth noting that the setting/stiffening of WGP-incorporated paste was still faster than that of pure cement paste. Also, the interval between the initial and final set was reduced significantly (41.4%). As the WGP with a low reactivity would not be involved in the hydration at this early age, the enhancement of the setting was largely ascribed to the accelerating cement hydration by SW. The benefit of SW was also reported by Etxeberria et al. [57], who found that the use of SW in combination with blast-furnace slag cement in concrete could achieve similar setting times to conventional concrete prepared with Portland cement. Therefore, via the combined use of SW and SCMs in the cement system, the delayed

hardening would be mitigated.

3.2 Macro and micro mechanical properties

The early compressive strength of cement mortar at 1 and 3 days are presented in Fig. 11. In the case of the control mortar, the compressive strengths were enhanced largely by using SW in lieu of FW. In particular, a much higher increase of 1-day strength could be observed when compared with the increase of 3-day strength. Fig. 11b shows that the contribution of SW to the 1-day strength was 42.8% while only 10.7% increase was resulted from SW for the 3-day strength. These results indicate that the accelerating effect of SW on the strength was more pronounced at the early stage.

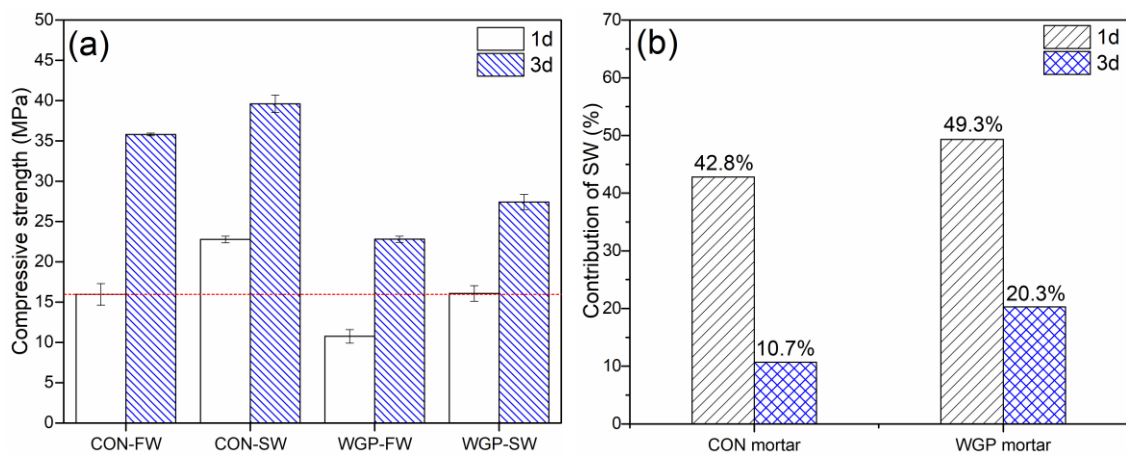


Fig. 11. Early strength of control and WGP mortars prepared with FW and SW: (a) Compressive strength (b) Contribution of SW.

When the WGP was introduced to replace cement, the strength of the cement mortar was reduced obviously, regardless of 1 day and 3 days of curing. This confirms that the WGP had a very low pozzolanic activity at the early ages [18]. However, the use of the WGP in combination with the SW notably increased the early strength, especially for the 1-day strength. As indicated in Fig. 11b, by using SW, approximate 50% and 20% of WGP-mortar strengths were added to the 1-day and 3-day strengths, respectively. It is worth to notice that, in the case of the WGP blended mortar prepared with SW, the compressive strength at 1 day was comparable to the corresponding strength of the control mortar prepared with FW. These findings imply that the combined use of the WGP and the SW was effective in overcoming the dilution effect by the WGP inclusion at the very early age.

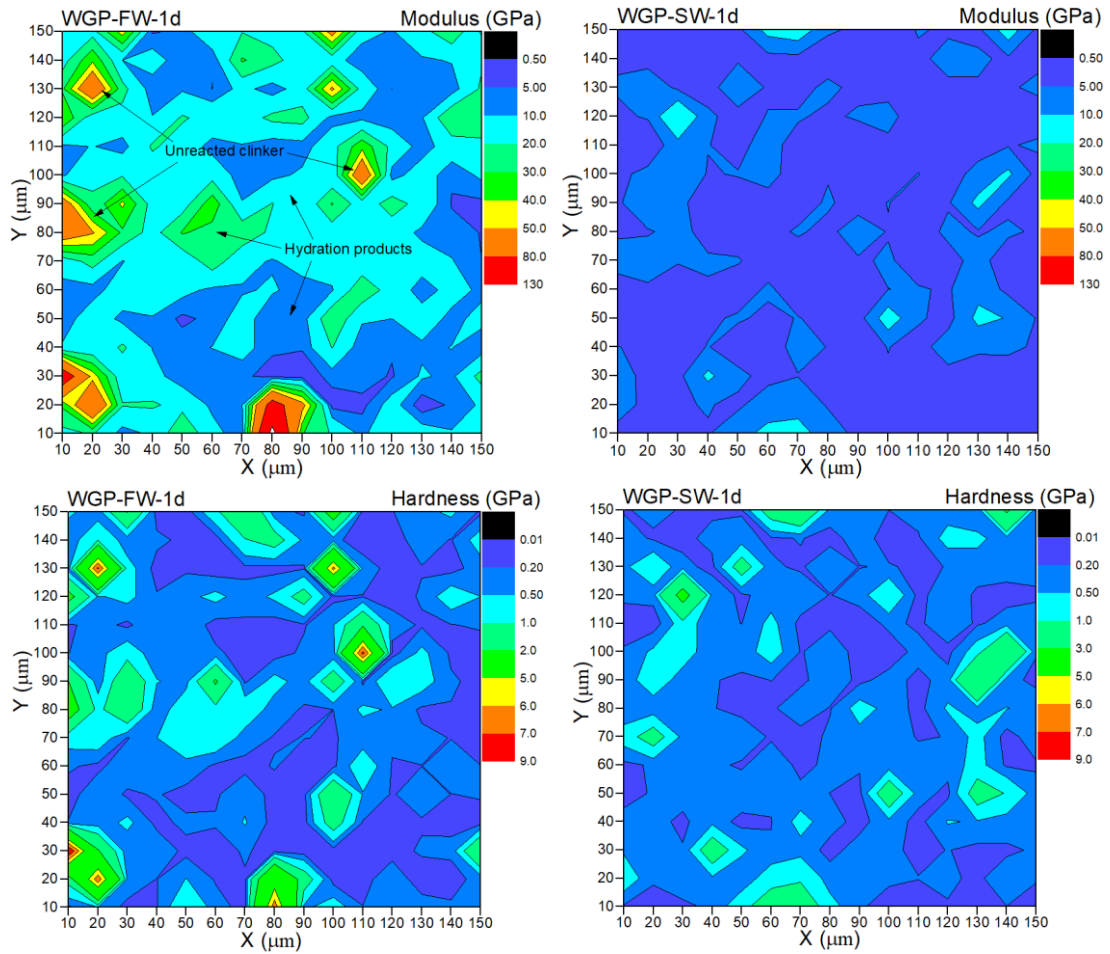


Fig. 12. Contour maps of elastic modulus and hardness of WGP pastes prepared with FW and SW at 1 day.

In order to further understand the effectiveness of SW in improving the early strength of WGP-incorporating mortars, the nanoindentation technique was adopted to assess the micromechanical properties of the WGP blended paste prepared with FW and SW. Fig. 12 presents the distributions of elastic modulus and hardness of WGP pastes mixed with FW and SW at 1 day. The high modulus and hardness values of some areas in the WGP-FW paste suggest the presence of many unreacted particles. These particles were surrounded by hydration products with relatively lower moduli and hardness, which means that these particles were unhydrated clinker phases rather than glass particles. In contrast, no obviously unreacted clinker particles were observed in the WGP blended paste mixed with SW, indicating the accelerating dissolution of the clinker phases in the SW system. Since the C-S-H is the dominant product in the hydrates and makes primary contribution to the strength, the hardness as a function of modulus of the C-S-H were analyzed for these two pastes. Generally, the elastic modulus and hardness of the C-S-H phases were within 35 GPa and 1.5 GPa, respectively, from the statistical nanoindentation technique [58]. With this region in Fig. 13, higher modulus values of C-S-H

gel were basically found in the WGP paste mixed with FW, whereas higher hardness values of C-S-H gel were observed in the SW mixed WGP paste under the same level of hardness/modulus. As the hardness is typically related to the mechanical properties based on the definition equation [58], the higher hardness of C-S-H gel was believed to contribute to the higher strength of WGP-SW sample in comparison with the WGP-FW sample.

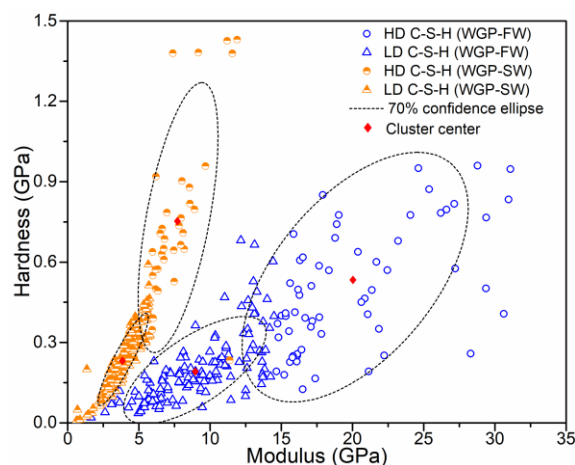


Fig. 13. Deconvolution of clustered C-S-H properties of the WGP pastes prepared with FW and SW at 1 day.

Two types of C-S-H are present in cementitious materials, namely, a low-density (LD) form and a high-density (HD) form [59]. To obtain quantitative information of the C-S-H phases, a statistical deconvolution was conducted to identify the two categories of the C-S-H gel according to Gaussian mixture modelling. Confidence ellipse at confidence level of 70% was also performed for the different clusters of C-S-H based on the Gaussian distribution. The clustered data and the confidence ellipse of the LD/HD C-S-H are shown in Fig. 13 by deconvolution method [60]. Also, the data of the corresponding cluster centers can be obtained to represent the typical properties of the LD and HD C-S-H in the WGP pastes mixed with FW and SW. The modulus and hardness of the LD and HD C-S-H are presented in Table 5. As seen, the elastic modulus was much lower in the WGP-SW paste as compared to that in the WGP-FW paste, regardless of the LD and HD C-S-H gels. However, the hardness of the LD and HD C-S-H gels in the former was higher than that of later. These results are in good agreement with the above qualitative observations. The modulus is mainly dependent on the intrinsic properties of materials [61], which means that the presence of SW changed the structure of the C-S-H. The reason may be assigned to the fact that the presence of Mg^{2+} cations in the SW would influence the modulus of the C-S-H. The presence of Mg^{2+} in the system could lead to the decalcification of Ca^{2+} from C-S-H [62], which probably caused the deterioration in the modulus of C-S-H. Also, the magnesium silicate hydrates (M-S-H) formed [62] provided less

stabilization of the matrix than the C-S-H [63]. The increased hardness in the SW system was likely attributed to the denser C-S-H matrix due to the formation of larger amount of C-S-H. Regarding the cementitious materials mixed with SW, more studies need to be performed to understand the mechanism on the nanostructure changes of C-S-H phases.

Table 5. Properties of C-S-H in the WGP pastes prepared with FW and SW (Cluster center).

C-S-H	Properties	WGP-FW	WGP-SW
LD	Modulus (GPa)	8.94	3.90
	Hardness (GPa)	0.20	0.24
HD	Modulus (GPa)	20.17	7.77
	Hardness (GPa)	0.54	0.77

3.3 Early hydration

Fig. 14 shows the hydration heat evolution profiles of the cement pastes upon mixing with FW and SW. As demonstrated in Fig. 14a, at the very early age of hydration, the SW pure cement paste mixed released a much higher amount of heat than the FW paste. As the cations (e.g. Na^+ and Mg^{2+}) in the SW tended to accelerate the dissolution of C_3S [55], so that the use of SW was able to expedite the precipitation of hydration products (i.e. C-S-H and portlandite) and speed up the very early hydration.

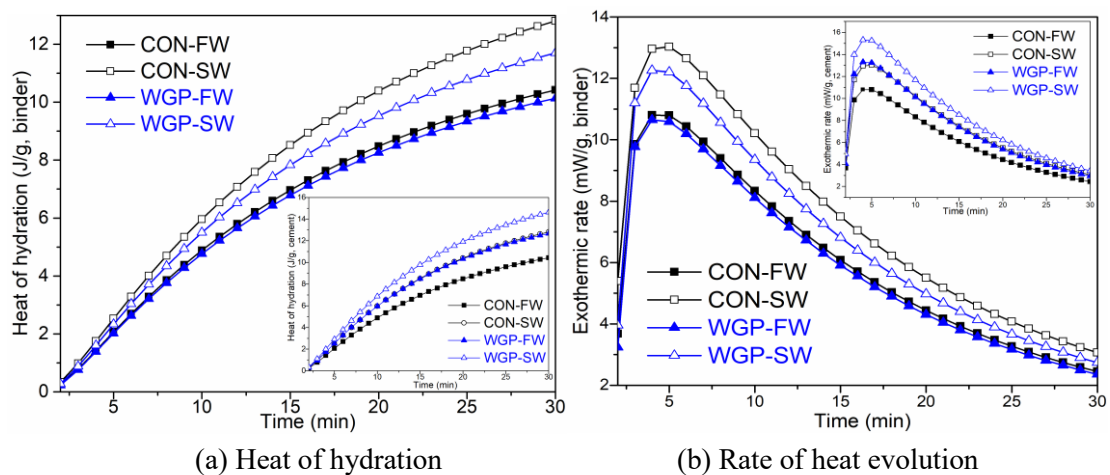


Fig. 14. Heat evolutions of control and WGP pastes prepared with FW and SW within first 30 min (the inserts are normalized by mass of cement, g).

The results showed that the cement paste blended with WGP produced a slightly lower amount of heat than the control paste. This was due to the dilution effect and the lower reactivity of WGP. However, from the insert diagram in Fig. 14a (normalized by mass of cement), it can be noticed that the inclusion of WGP promoted the hydration of cement remarkably at this early age. Three factors might be responsible for this: 1) the higher effective w/c ratio caused

by the inclusion of WGP would increase the hydration degree of cement; 2) the WGP particles provide additional nucleation sites for the precipitation of cement hydration products; 3) the hydrolysis of the WGP particles.

The dissolution of the WGP in the FW and SW were monitored. Fig. 15a shows the increased pH (OH^- concentration) of solution by adding WGP in FW and SW. Such an increase of hydroxyl ion concentration is believed to be associated with the partial hydrolysis of very fine WGP particles during the first minutes of contact with water [50]. Afterwards, the pH was stabilized. The pH profile of the solution followed a similar trend with the evolution of Na concentration as shown in Fig. 15b. Therefore, due to the incorporation of the WGP, the changed pH environment and alkali concentration in the solution would inevitably affect the hydration of cement [51]. According to the studies of Mota et al. [64], the presence of NaOH in the solution could accelerate the hydration of cement during the early age (first hours). The increased dissolution of silicates (C_3S and C_2S) and enhanced precipitation of hydrated phases were responsible for the early accelerating effect by the alkali [65, 66]. Besides, a certain amount of silica in the WGP tended to dissolve in high pH pore solution [15]. Hence, the dissolved ions from WGP were conducive to promoting the hydration of cement so that the total heat liberation of the WGP paste was similar to that of the control paste. In Figs. 14a and 14b, the combined use of WGP and SW further favored the hydration. The insert of Fig. 14b also shows that the joint use of the WGP and SW assisted the cement to produce the highest heat flow, which was mainly attributed to the dual acceleration effects from the use of WGP and SW.

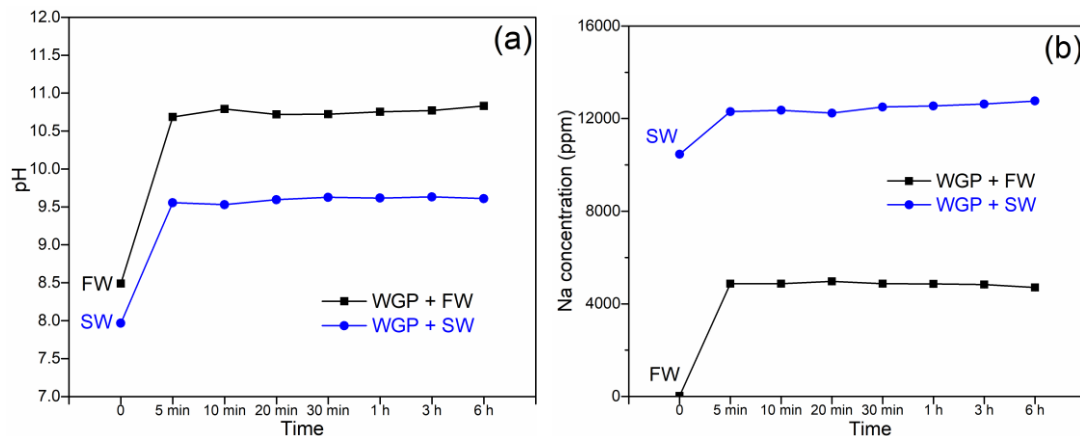


Fig. 15. Dissolution of the WGP in the FW and SW; (a) pH and (b) Na concentration.

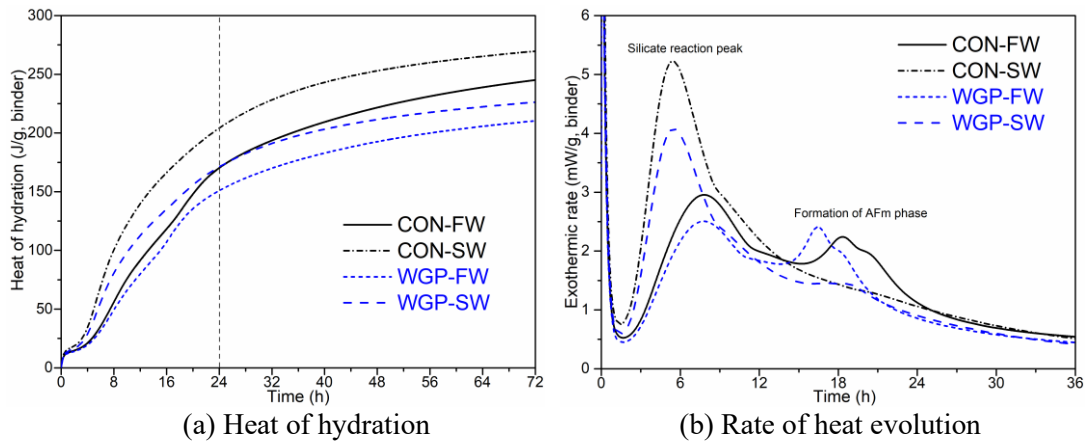


Fig. 16. Heat evolutions of control and WGP pastes prepared with FW and SW (up to 72 h).

Besides the very early heat of hydration (within 30 min), the heat evolutions (up to 72 h) of the WGP blended paste prepared with FW and SW were monitored and are shown in Fig. 16. Fig. 16a shows that the pure cement paste prepared with SW released much more heat as compared to the paste prepared with FW. When the WGP was used to partially replace cement, the heat output of the paste was reduced. The diluted cement content predominately resulted in the reduction of heat. After mixing the WGP cement with SW, the heat release of the paste was largely enhanced, especially for the 1-day hydration. The enhancement of the hydration contributed to promoting the development of mechanical properties (see Fig. 11). It is particularly worth pointing out that the cumulative amounts of heat released by the WGP-SW paste and CON-FW paste at 24 h were similar, which closely corresponded to their similar strength at the same age (1 day). This behavior suggests that the development of compressive strength might be correlated with the heat of hydration. To validate this hypothesis, their relationship is depicted in Fig. 17, which shows a well linear match between the compressive strength and the heat of hydration of the pastes at the early ages of hydration.

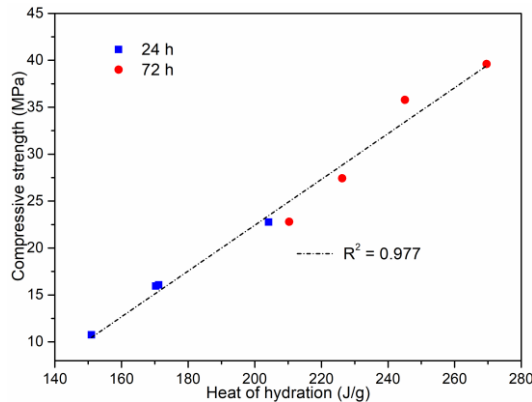
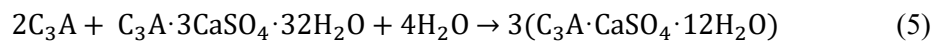


Fig. 17. Relationship between compressive strength and heat of hydration.

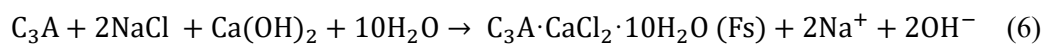
A closer examination was made on the heat flow of the pastes prepared by using FW and SW

in Fig. 16b. As compared to the control paste prepared with FW, the SW paste exhibited a more intensive and earlier second peak, which is mainly interpreted as the hydration of the silicate phase (C₃S). This means that the use of SW accelerated the dissolution of C₃S. The statement is confirmed by a recent study [55], which indicated that the use of SW enhanced the Ca²⁺ concentration and participation of hydration products (portlandite and C-S-H) in the acceleration period of C₃S hydration. The same accelerating behavior was also noticed in the case of WGP blended paste mixed with SW. The incorporation of WGP decreased the silicate reaction peak because of the cement dilution, however, the duration of the induction and acceleration periods did not change significantly. In contrast, the use of SW shortened the induction period and speeded up the acceleration period, which contributed to the faster stiffening of the paste. Therefore, the setting times of the SW pastes were reduced (see Fig. 10).

Moreover, for the FW pastes, an apparent third peak on the shoulder of deceleration period was observed in the heat evolution profile of the control and WGP-contained paste, which is related to the formation of monosulfoaluminate (AFm, C₃A·CaSO₄·12H₂O) as a result of the reaction between the ettringite (AFt, C₃A·3CaSO₄·32H₂O) and the remnant of C₃A (as shown in Eq. 5) [67]. A similar phenomenon was also reported in previous works when white cement was employed as the binder [3, 14]. In this study, the lower content of gypsum in the cement (see Table 1) might have been completely consumed by the C₃A to form ettringite, thus a plentifully residual C₃A was present in the system to favor the conversion from AFt to AFm (Eq. 5). Moreover, the introduction of WGP brought the third peak to an earlier time. This is because the higher effective water content in the WGP paste would accelerate the secondary hydration of C₃A [3].



When using SW, no third peak was found in the pure cement paste. However, for the WGP blended paste prepared with the SW, the formation of the AFm phase was found to be weakened and delayed. A possible reason was that chloride ions in the SW bounded with part of the aluminate phase to form Friedel's salt (Fs, C₃A·CaCl₂·10H₂O) [68] (Eq. 6), so that there was insufficient C₃A remaining to produce the AFm phase (to be discussed in the following section).



3.4 Microstructural analyses

3.4.1 Mineralogy and morphology analyses

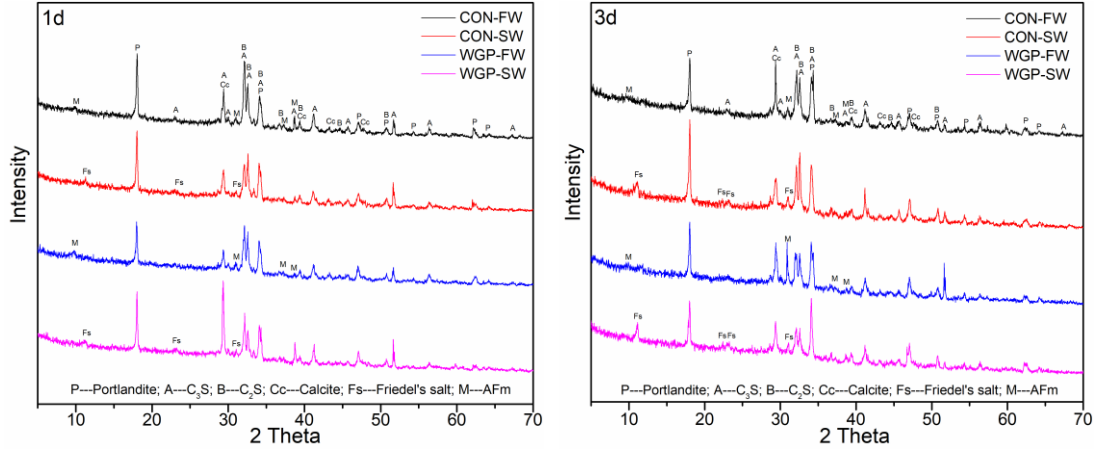


Fig. 18. XRD patterns of control and WGP pastes prepared with FW and SW at 1 d (left) and 3 d (right).

The XRD patterns and quantitative results (Q-XRD) of the crystalline phases are shown in Fig. 18 and Table 5, respectively. After 1-day curing, the unhydrated clinker minerals were still identified in the control FW paste. The main hydration product detected was portlandite (CH), and AFm phase. An appreciable difference in the SW paste was the presence of Friedel's salt (Fs). The formation of Fs was due to two mechanisms: a) dissolution and precipitation (Eq. 6) [69], and b) anion exchange (Eq. 7) [70]. Eq. 6 suggests that the formation of Fs could be triggered at the early age of hydration with the dissolution of the aluminate phase. Furthermore, based on Eq. 7, the formed hydroxy-AFm phase could react with chloride to form Fs by the ion exchange between SO_4^{2-} and Cl^- , thus the typical diffraction peaks of AFm in the 1 day control paste disappeared when using SW. The same phenomenon also occurred in the WGP blended pastes mixed with SW. When the WGP was used to partially replace cement, the content of CH was reduced as listed in Table 6. This may be due to the reduction in cement content of the paste. However, it is noticed that using SW in WGP-based mixture increased the CH amount, which suggests the accelerated hydration by the SW. This was also evidenced in the case of SW pure cement paste, which had a larger amount of amorphous phase (C-S-H) and CH as compared to the control FW paste.

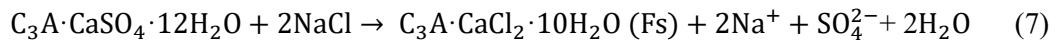


Table 6. Crystalline phases in pastes by Q-XRD.

Phases	1d				3d			
	CON-FW	CON-SW	WGP-FW	WGP-SW	CON-FW	CON-SW	WGP-FW	WGP-SW
C ₃ S	15.9	11.6	10.8	11.0	9.9	8.8	7.3	7.7
C ₂ S	19.3	18.6	15.6	14.4	19.0	15.2	14.7	12.8
C ₃ A	1.5	1.7	0.9	1.4	0.5	0.8	0.4	0.5
Gypsum	0.9	0.7	0.7	1.4	0.9	1.5	0.9	1.2
CH	5.6	6.7	4.7	7.5	7.2	8.2	6.2	8.9
Calcite	7.9	8.0	5.7	5.0	7.1	8.0	7.1	6.6
AFm	2.0	-	0.7	-	1.2	-	0.3	-
AFt	1.5	-	0.3	-	0.2	-	0.4	-
Fs	-	0.8	-	1.2	-	3.3	-	3.8
Amorphous	45.5	51.9	60.6	58.2	54.0	54.2	62.7	58.6

Note: ‘-’ means undetectable phases, the R_{wp} of the Q-XRD results was refined to about 10% based on Rietveld refinement.

After 3 days of curing, there were still many unreacted clinker materials being detected in the FW pure cement paste. As compared to 1-day sample, the 3-day SW pure cement paste prepared contained a larger amount of Friedel’s salt (Fs). A similar behavior was also observed in the WGP blended SW. However, for the SW samples, the Fs content in the WGP blended paste was higher than that in the pure cement paste. This is probably attributed to more chloride ions were available in the pore solution and involved in the reactions of Eqs. 6 and 7 due to the increased w/c ratio in the WGP-SW paste. Hence, the large-sized crystalline Fs could be found (a classic petal-like hexagonal sheet structure) in the WGP-SW paste (Fig. 19a).

An interesting phenomenon was found in the Q-XRD results that the use of SW resulted in more C₃A remaining in the pastes, which means that SW appeared to suppress the hydration of C₃A to some extent. This is confirmed by the higher amount of remnant gypsum in the SW pastes. The reason can be probably explained by chloride ions preferentially react with the C₃A phase, because the mobility of Cl⁻ was higher than the SO₄²⁻ due to the ion valences and molecular sizes (Cl⁻ < SO₄²⁻) [71, 72]. It had been reported that the higher the mobility of anions, the faster was the reaction [54]. Therefore, the use of SW would interfere with AFt and AFm crystallizations, which corresponds to the very low amount of AFt and AFm detected in the SW-containing pastes (Table 6). A similar phenomenon was found in the cement mortar

exposed to the solution containing chloride and sulfate ions [73], indicating that the presence of Cl^- could reduce the formation of ettringite since partial C_3A was combined as Fs. The reduced contents of calcium sulfoaluminate hydrates are also in line with the weakening formation of AFm phase in the hydration results (Fig. 16b). The relatively high content of calcite may be due to the carbonation during sample preparation as the early age structure of paste was quite loose.

When a hardened cement-based material is exposed to a saline solution such as SW, the precipitation of crystalline Fs is thought to engender a weakening in the mechanical properties due to the crystallization stresses in the pores [74]. However, in this study, the saline SW was prepared and mixed with the cementitious materials right at the beginning, and the formation of Fs started at the early ages (within 15 min of hydration [68]). As indicated in a previous study [75], the mixing of chloride salt with a slag cement produced hexagonal plates of Fs that was found to reduce the pore size and densify the matrix. Another work [76] also suggested that by mixing brine water with steel slag, the concomitant presence of Fs and C-S-H gels was thought to contribute to strength. Therefore, it is inferred that the Fs formed at the early age would exert a different role with the ingress of chloride ions from external environment (i.e. the occurrence of Fs at the later age). The morphologies of the pastes prepared with WGP and SW were observed by SEM, and the images are presented in Figs. 19b and c. It can be seen that the Fs was formed randomly together with CH in the WGP-SW paste. The compositional differences of the Fs and the CH are depicted in Fig. 19d, showing that Al and Cl were present in Fs (calcium chloro-aluminate hydrate). The Fs crystals formed at the early age were able to integrate with other hydration products in the SW mixture to block the pores and favored the enhancement of the early strength.

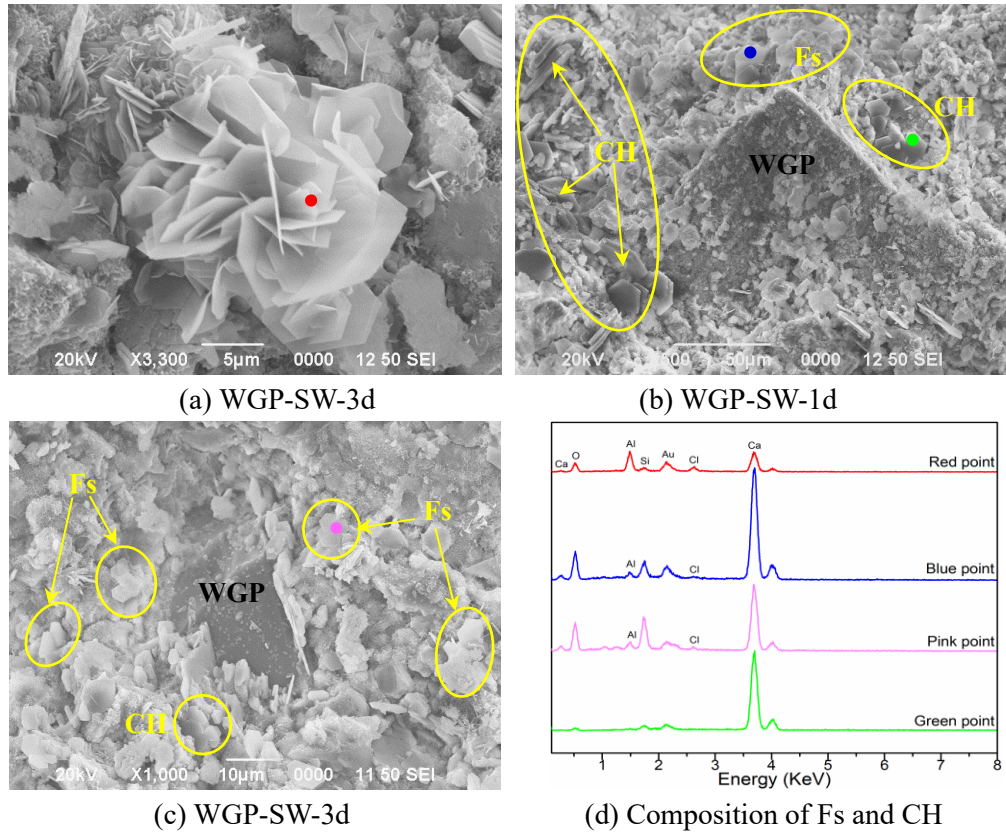


Fig. 19. Morphology and EDX of the WGP pastes prepared with SW.

3.4.2 Thermogravimetric analysis

The TG and DTG results are shown in Fig. 20. The 3-day samples exhibited a higher mass loss compared to the 1-day samples, and all the paste samples experienced three main mass loss peaks. It is generally accepted that these three peaks correspond respectively to the loss of free water/bound water in the hydrates (C-S-H, ettringite and monosulfate phases), dehydroxylation of portlandite and decarbonation of carbonates [46]. In particular, Fig. 20b shows tiny shoulder peaks at around 140 °C present in the FW mixed pastes, which was probably ascribable to the dehydration of AFm phases [77] as the SW pastes did not have these dehydration peaks. Instead, small endothermic peaks at 250–350 °C were observed in the SW-containing pastes but not in the FW pastes. This temperature region had been considered to be associated with the loss of main-layer water in Fs [46], which further validates the conversion of aluminat phases to Fs in the presence of SW.

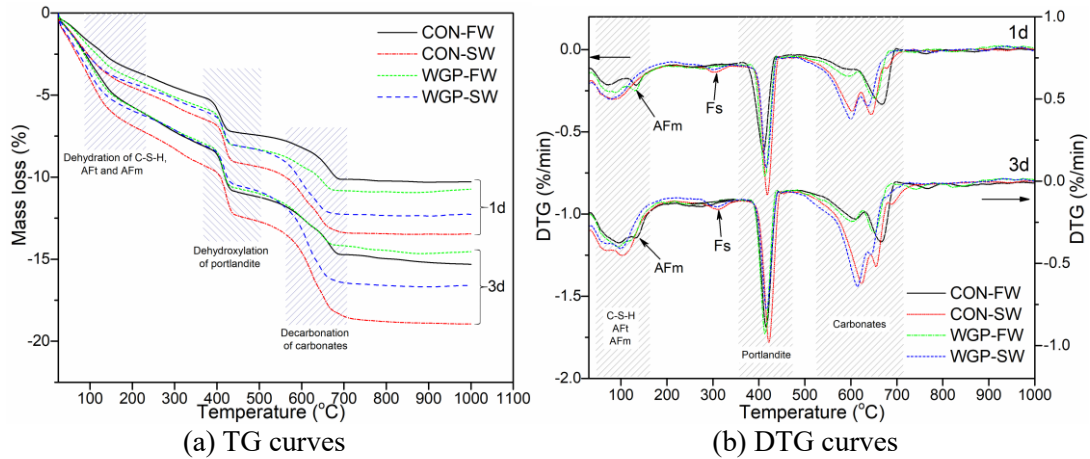


Fig. 20. Thermal analyses of the control and WGP pastes prepared with FW and SW.

The significant weight loss peaks above 400 °C were indicative of the dehydroxylation of CH. Decarbonation was seen at the temperature range of 550–700 °C. Several peaks related to the decomposition of C-S-H carbonates also had been observed in other hydrated Portland cement [46, 78]. It is known that CaCO_3 has three polymorphs (calcite, vaterite and aragonite) [79]. But no aragonite and vaterite crystals were identified in the XRD patterns of this study, which means that calcite was the main phase of calcium carbonate present. Stepkowska [80] indicated that smaller size calcite decomposed at a lower temperature while CO_2 would escape from the larger monocrystalline calcite at a higher temperature. Furthermore, the crystallinity of carbonate crystallites also affected the decarbonation temperature, i.e. the poorly crystallized calcite is decomposed at below 600 °C and well crystallized calcite is decomposed at above 600 °C [81]. Therefore, it is believed that these two endothermic peaks at 550–700 °C were associated with the decompositions of different sizes and/or crystallinities of calcium carbonates [82].

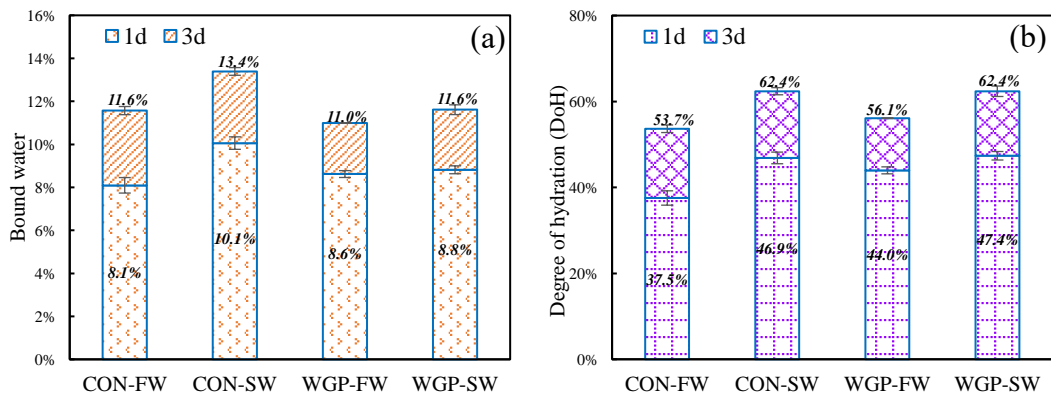


Fig. 21. Chemically bound water (a) and degree of hydration (b) of control and WGP pastes prepared with FW and SW.

Fig. 21 shows the values of the measured chemically bound water and corresponding DoH of

the cement pastes. From Fig. 21a, a higher content of bound water in the SW paste can be noted, which further confirmed the accelerated dissolution of the clinker minerals and precipitation of hydration products with the use of SW. Unexpectedly, the amounts of bound water in the 1-d pastes prepared with WGP and FW were higher than that in the control paste. One explanation was the higher effective w/c ratio and dissolved alkali ions due to the presence of WGP which promoted the cement hydration. However, an opposite trend occurred after 3-d because the dilution effect dominated the amount of hydrates that would be produced.

In this study, cement pastes prepared with the same proportions and cured for four years were used to obtain the amount of bound water at complete hydration as references. The amount of the bound water in the four-year-old CON-FW, CON-SW, WGP-FW and WGP-SW paste was 21.6%, 21.5%, 19.6% and 18.6%, respectively. The bound water content of the pure cement paste appeared to closely match with the study of Bhatta [83], who reported that the amount of bound water in a fully hydrated cement paste was 21.0% by mass of cement. Therefore, the bound water contents of the four years old cement paste seemed to be reasonable references for estimating the degree of hydration (DoH) in this study. As indicated in Fig. 21b, since the SW pure paste had similar bound water contents to the FW pure paste at long-term age, thus the DoH of the former at the early age was much larger due to the enhancement of hydration by SW. It is interesting to note that the DoH of the WGP-incorporated paste was higher than that of the control paste. This behavior is in agreement with the findings of Berodier and Scrivener [84], and Lawrence et al. [85], where they found that the DoH of the neat cement paste/mortar within the first 3 day of hydration was lower than the paste/mortar blended with an inert quartz powder. One of the reasons for this phenomenon was that the reduced amount of cement by WGP replacement decreased the bound water of the hydrates at the later day of hydration. Furthermore, the incorporation of WGP was able to promote the remaining cement hydration as mentioned above. It is also observed that the DoH of the paste prepared with WGP and SW was higher than that of the paste incorporating WGP alone and similar to that of the SW mixed neat paste. The accelerated hydration due to the use of SW and the relatively smaller amount of bound water at full hydration were mainly responsible for the increased value.

3.4.3 Pore structure analysis

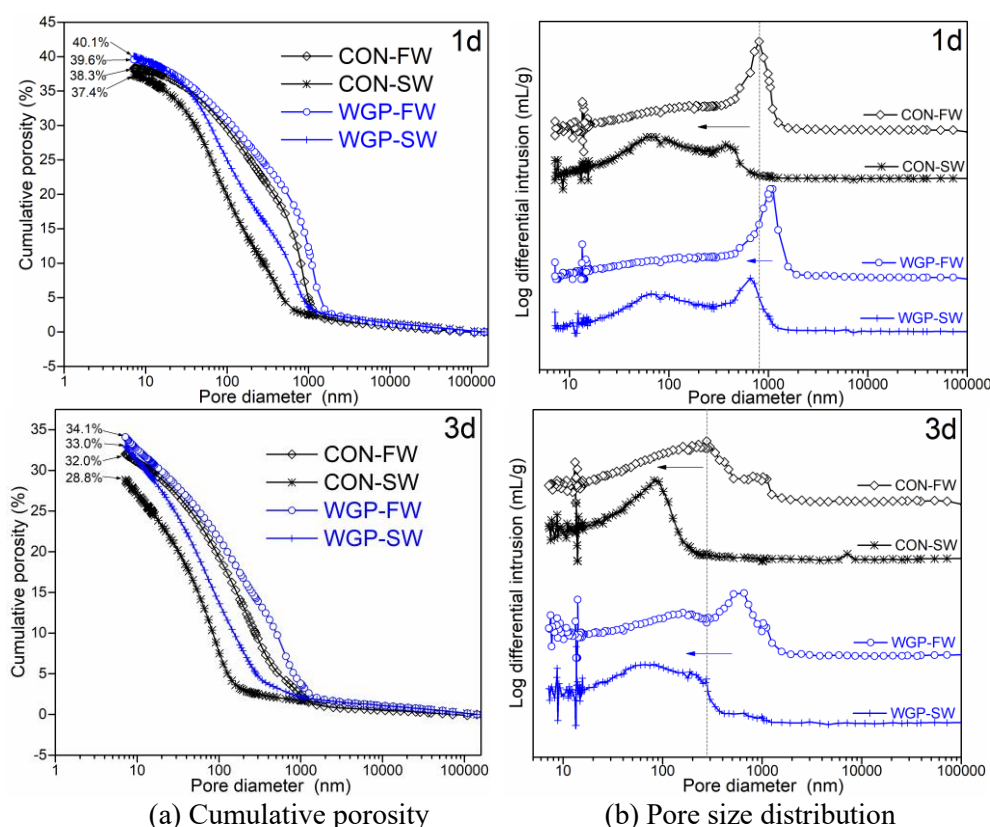


Fig. 22. Pore structures of control and WGP pastes prepared with FW and SW.

As demonstrated in Fig. 22a, the use of SW reduced the porosity of the matrix as compared to the FW mix, especially for the 3-day samples. Since the pore structure plays a crucial role in determining the strength of cement-based materials, the reduction of porosity by SW was mainly responsible for the enhancement of the early strength, which agrees with the results of mechanical properties tests. It is also found that the incorporation of WGP increased the cumulative porosity of the mixture (as shown in Table 7), irrespective of 1 day or 3 days curing. The reasons can be explained by the increase of effective w/c ratio and reduced cement content due to the replacement of cement by WGP. Another possibility is that the reduced workability and higher viscosity of WGP incorporated mixture resulted in inferior compaction (see Section 3.1). Fig. 22b shows the variation of incremental mercury intrusion as a function of the pore size diameter in the cement pastes. Comparing the FW and SW 1-d pure cement pastes, the narrow critical pore peak of the FW pastes moved toward the left and turned into broad hump in the SW pastes, which means a refinement of the pore size. This effect was more pronounced in the 3-day pastes. As indicated in Table 7, the critical pore size and the median pore diameter were considerably reduced in the SW pastes.

Table 7. Characteristics of pore structure by MIP.

Age	Mix	Cumulative porosity (%)	Critical pore diameter (nm)	Median pore diameter (volume, nm)
1d	CON-FW	38.3	808.2	417.6
	CON-SW	37.4	66.5	110.1
	WGP-FW	39.6	1109.8	572.8
	WGP-SW	40.1	660.6	170.1
3d	CON-FW	32.0	277.3	147.9
	CON-SW	28.8	66.5	58.7
	WGP-FW	34.1	516.9	189.7
	WGP-SW	33.0	82.4	75.4

The inclusion of WGP coarsened the pore size of the matrix at the early ages. Therefore, the WGP-based mortar exhibited a lower strength as compared to the control mortar. Nonetheless, Fig. 22 shows that the combined use of WGP and SW shifted the pore size distribution towards the finer size. It is interesting to note that, in Table 7, the paste prepared with WGP in conjunction with SW had much smaller critical and median pore diameters than the control paste made with FW. A positive contribution is expected from the refinement of the pore size on the strength development of the mortar in Section 3.2. In order to quantitatively character the pore-refining effect by using SW in the WGP paste, a classification of pore structure was suggested at four ranges: 7-50 nm (mesopores), 50-200 nm (small capillary pores), 200-1000 nm (medium capillary pores), >1000 nm (large capillary pores). From Fig. 23, it is clear that the use of SW significantly increased the volume fractions of mesopores and small capillary pores for both the neat paste and the WGP-incorporated paste. The combined use of the WGP and the SW could refine the medium and large capillary pores into small mesopores and capillary pores in comparison with the use of WGP alone. This benefit implies that the use of SW in WGP-incorporated mixture could counteract the pore-coarsening effect caused by the WGP inclusion at the early age.

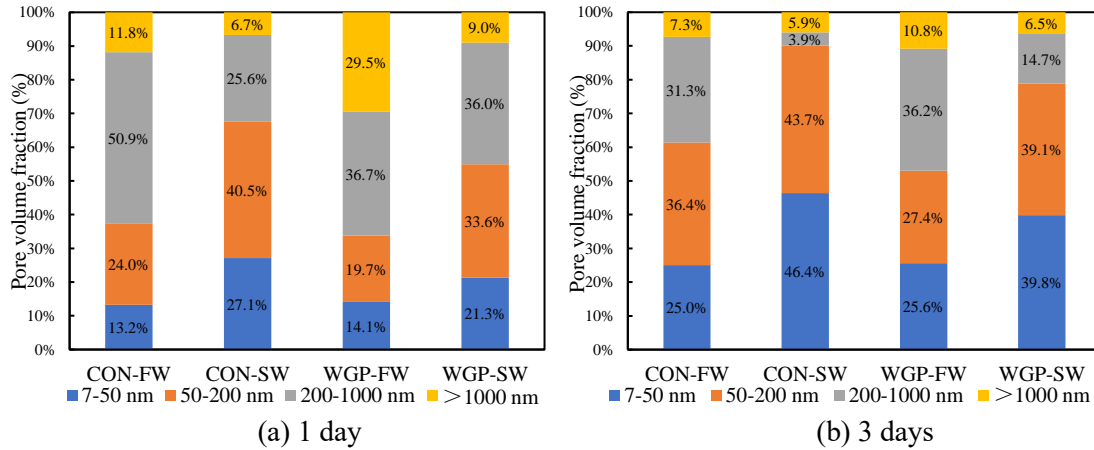


Fig. 23. Pore volume fraction of control and WGP pastes prepared with FW and SW.

4 Conclusion

In this study, SW was used as mixing water to improve the early age properties of cementitious materials prepared with a low reactivity SCM (i.e. WGP). The effectiveness of combined use of SW and WGP in rheological behaviors, macro and micro-scale mechanical properties and early hydration of cement paste or mortar were evaluated and analyzed. The mechanisms on improving the early age and microstructural performance were discussed in the light of Q-XRD, morphology observation, thermal decomposition and pore structure measurements. The following conclusions can be drawn:

- The use of SW increased the dynamic yield stress and plastic viscosity of cement pastes due to the acceleration of cement hydration. However, the yield stress and plastic viscosity of the WGP blended paste at the early age were primarily affected by the physicochemical properties of WGP, such as its fine particle size, negative surface charge and the ion dissolution from the WGP. Due to the synergetic effects of SW and WGP, the viscosity of the blended cement paste was further increased.
- The higher viscosity of the WGP blended paste resulted in the reduction of flow. The setting times were delayed when the WGP was incorporated due to the increased effective w/c ratio and low reactivity of WGP. However, the combined use of SW was effective in shortening the setting times.
- The use of WGP led to a significant reduction in the early strength, whereas the combined use of WGP and SW could compensate for the strength loss. The nanoindentation results indicated that the use of SW produced C-S-H with higher hardness in the WGP-SW system, which may contribute to the higher strength.
- Dissolved ions from WGP were conducive to accelerating the hydration of cement.

With the joint use of SW, the heat release of the paste was largely increased, especially for the first day of hydration. The accelerated hydration favored the development of early strength, which was validated by the linear relationship between the heat liberation and strength.

- The Q-XRD and TG results indicated that using SW with WGP blended paste facilitated the dissolution of the clinker phases and the precipitation of hydration products. In particular, the formation of Fs was found in the SW mixed mixture instead of AFt and AFm. The Fs formed might be able to refine the pores and increase the early strength. The combined use of WGP and SW increased the degree of hydration of mixture at the early age and alleviate the pore-coarsening impact caused by the WGP inclusion in the paste at the early age.

Acknowledgement

The authors gratefully acknowledge the financial support of the Research Grants Council Theme-based Research Scheme (Project No. T22-502/18-R) and the Hong Kong Polytechnic University. The technical assistances of Ms. Dorothy Chan and Ms. Celine Che (laboratory technician in the Department of Civil and Environmental Engineering) in carrying out the MIP and zeta potential tests are gratefully acknowledged. Thanks are also due to Mr. Yazan Alrefaei, Mr. Hafiz Asad Ali, and Mr. Yi Jiang for their assistances in performing the rheology and ion concentration measurements.

References

- [1] B. Lothenbach, K. Scrivener, R.D. Hooton, Supplementary cementitious materials, *Cement and Concrete Research*, 41 (2011) 1244-1256.
- [2] M.C.G. Juenger, R. Siddique, Recent advances in understanding the role of supplementary cementitious materials in concrete, *Cement and Concrete Research*, 78 (2015) 71-80.
- [3] J.-X. Lu, Z.-H. Duan, C.S. Poon, Combined use of waste glass powder and cullet in architectural mortar, *Cement and Concrete Composites*, 82 (2017) 34-44.
- [4] J.-X. Lu, B.-J. Zhan, Z.-H. Duan, C.S. Poon, Using glass powder to improve the durability of architectural mortar prepared with glass aggregates, *Materials & Design*, 135 (2017) 102-111.
- [5] HK Environmental Protection Department, Monitoring of Solid Waste in Hong Kong, Waste Statistics, (1997-2017) https://www.wastereduction.gov.hk/en/assistancewizard/waste_red_sat.htm.
- [6] J.-X. Lu, C.S. Poon, Recycling of waste glass in construction materials, In: *New Trends in Eco-efficient and Recycled Concrete*, (2019) 153-167.
- [7] Y. Jiang, T.C. Ling, K.H. Mo, C. Shi, A critical review of waste glass powder - Multiple roles of utilization in cement-based materials and construction products, *Journal of environmental management*, 242 (2019) 440-449.
- [8] S. Chandra Paul, B. Šavija, A.J. Babafemi, A comprehensive review on mechanical and durability

- properties of cement-based materials containing waste recycled glass, *Journal of Cleaner Production*, 198 (2018) 891-906.
- [9] M.N.N. Khan, A.K. Saha, P.K. Sarker, Reuse of waste glass as a supplementary binder and aggregate for sustainable cement-based construction materials: A review, *Journal of Building Engineering*, 28 (2020) 101052.
- [10] J.-X. Lu, P. Shen, H. Zheng, H.A. Ali, C.S. Poon, Development and characteristics of ultra high-performance lightweight cementitious composites (UHP-LCCs), *Cement and Concrete Research*, 145 (2021) 106462.
- [11] H. Du, K.H. Tan, Properties of high volume glass powder concrete, *Cement and Concrete Composites*, 75 (2017) 22-29.
- [12] H. Siad, M. Lachemi, M. Sahmaran, K.M.A. Hossain, Effect of glass powder on sulfuric acid resistance of cementitious materials, *Construction and Building Materials*, 113 (2016) 163-173.
- [13] H. Du, K.H. Tan, Transport properties of concrete with glass powder as supplementary cementitious material, *ACI Materials Journal*, 112 (2015).
- [14] J.-X. Lu, Z.-H. Duan, C.S. Poon, Fresh properties of cement pastes or mortars incorporating waste glass powder and cullet, *Construction and Building Materials*, 131 (2017) 793-799.
- [15] M. Mirzahosseini, K.A. Riding, Influence of different particle sizes on reactivity of finely ground glass as supplementary cementitious material (SCM), *Cement and Concrete Composites*, 56 (2015) 95-105.
- [16] C. Shi, Y. Wu, C. Riefler, H. Wang, Characteristics and pozzolanic reactivity of glass powders, *Cement and Concrete Research*, 35 (2005) 987-993.
- [17] H.A. Elaqla, M.A.A. Haloub, R.N. Rustom, Effect of new mixing method of glass powder as cement replacement on mechanical behavior of concrete, *Construction and Building Materials*, 203 (2019) 75-82.
- [18] J.-X. Lu, C.S. Poon, Improvement of early-age properties for glass-cement mortar by adding nanosilica, *Cement and Concrete Composites*, 89 (2018) 18-30.
- [19] Z. Chen, Y. Wang, S. Liao, Y. Huang, Grinding kinetics of waste glass powder and its composite effect as pozzolanic admixture in cement concrete, *Construction and Building Materials*, 239 (2020) 117876.
- [20] J. Xiao, C. Qiang, A. Nanni, K. Zhang, Use of sea-sand and seawater in concrete construction: Current status and future opportunities, *Construction and Building Materials*, 155 (2017) 1101-1111.
- [21] S. Cheng, Z. Shui, T. Sun, Y. Huang, K. Liu, Effects of seawater and supplementary cementitious materials on the durability and microstructure of lightweight aggregate concrete, *Construction and Building Materials*, 190 (2018) 1081-1090.
- [22] Q. Li, H. Geng, Z. Shui, Y. Huang, Effect of metakaolin addition and seawater mixing on the properties and hydration of concrete, *Applied Clay Science*, 115 (2015) 51-60.
- [23] S.K. Kaushik, S. Islam, Suitability of sea water for mixing structural concrete exposed to a marine environment, *Cement & Concrete Composites*, 17 (1995) 177-185.
- [24] Y.L. Li, X.L. Zhao, R.K. Singh Raman, Mechanical properties of seawater and sea sand concrete-filled FRP tubes in artificial seawater, *Construction and Building Materials*, 191 (2018) 977-993.
- [25] S. Soares, N. Freitas, E. Pereira, E. Nepomuceno, E. Pereira, J. Sena-Cruz, Assessment of GFRP bond behaviour for the design of sustainable reinforced seawater concrete structures, *Construction and Building Materials*, 231 (2020) 117277.
- [26] Y. Gao, Y. Zhou, J. Zhou, X. Kong, B. Zhang, S. Liu, J. Feng, N. Zhu, H. Fan, F. Jin, Blast responses

of one-way sea-sand seawater concrete slabs reinforced with BFRP bars, *Construction and Building Materials*, 232 (2020) 117254.

[27] Q. Zhang, J. Xiao, Q. Liao, Z. Duan, Structural behavior of seawater sea-sand concrete shear wall reinforced with GFRP bars, *Engineering Structures*, 189 (2019) 458-470.

[28] A. Zhou, R. Qin, C.L. Chow, D. Lau, Structural performance of FRP confined seawater concrete columns under chloride environment, *Composite Structures*, 216 (2019) 12-19.

[29] M. Etxeberria, J.M. Fernandez, J. Limeira, Secondary aggregates and seawater employment for sustainable concrete dyke blocks production: Case study, *Construction and Building Materials*, 113 (2016) 586-595.

[30] P. Li, W. Li, T. Yu, F. Qu, V.W.Y. Tam, Investigation on early-age hydration, mechanical properties and microstructure of seawater sea sand cement mortar, *Construction and Building Materials*, 249 (2020) 118776.

[31] J.-X. Lu, B.-J. Zhan, Z.-H. Duan, C.S. Poon, Improving the performance of architectural mortar containing 100% recycled glass aggregates by using SCMs, *Construction and Building Materials*, 153 (2017) 975-985.

[32] JCI, Technical Committee Report on the Use of Seawater in Concrete, Japan Concrete Institute, (2015).

[33] UNESCO World Water Assessment Programme, The United Nations world water development report 2019: Leaving no one behind, (2019) 1-11.

[34] ASTM C150/C150M-19a, Standard specification for portland cement, American Society of Testing Materials, (2019).

[35] J.-X. Lu, P. Shen, H. Zheng, B. Zhan, H.A. Ali, P. He, C.S. Poon, Synergetic recycling of waste glass and recycled aggregates in cement mortars: Physical, durability and microstructure performance, *Cement and Concrete Composites*, 113 (2020).

[36] R. Shaughnessy, P.E. Clark, The rheological behavior of fresh cement pastes, *Cement and Concrete Research*, 18 (1988) 327-341.

[37] BS EN 1015-3/A2, Methods of test for mortar for masonry - Part 3: Determination of consistence of fresh mortar (by flow table), British Standard Institution, (2007).

[38] GB/T 8077, Methods for testing uniformity of concrete admixture, National Standard of RPC, (2012).

[39] P. Domone, C. Hsi-Wen, Testing of binders for high performance concrete, *Cement and Concrete Research*, 27 (1997) 1141-1147.

[40] BS EN 196-3, Methods of testing cement Part 3: Determination of setting times and soundness, British Standard Institution, (2016).

[41] ASTM C109/C109M-20a, Standard test method for compressive strength of hydraulic cement mortars (Using 2-in. or [50-mm] cube specimens), American Society of Testing Materials, (2020).

[42] P. Mondal, S.P. Shah, L. Marks, A reliable technique to determine the local mechanical properties at the nanoscale for cementitious materials, *Cement and Concrete Research*, 37 (2007) 1440-1444.

[43] G. Pharr, A. Bolshakov, Understanding nanoindentation unloading curves, *Journal of Materials Research*, 17 (2002) 2660-2671.

[44] W.C. Oliver, G.M. Pharr, An improved technique for determining hardness and elastic modulus using load and displacement sensing indentation experiments, *Journal of Materials Research*, 7 (1992) 1564-1583.

[45] ASTM E1131-20, Standard test method for compositional analysis by thermogravimetry, American

- Society of Testing Materials, (2020).
- [46] K. Scrivener, R. Snellings, B. Lothenbach, A practical guide to microstructural analysis of cementitious materials, CRC Press, New York, USA, (2016).
- [47] J.I. Bhatti, K.J. Reid, Use of thermal analysis in the hydration studies of a type 1 portland cement produced from mineral tailings, *Thermochimica Acta*, 91 (1985) 95-105.
- [48] W. Deboucha, N. Leklou, A. Khelidj, M.N. Oudjit, Hydration development of mineral additives blended cement using thermogravimetric analysis (TGA): Methodology of calculating the degree of hydration, *Construction and Building Materials*, 146 (2017) 687-701.
- [49] ASTM D4404–10, Standard test method for determination of pore volume and pore volume distribution of soil and rock by mercury intrusion porosimetry, American Society of Testing Materials, (2010).
- [50] H.A. Elaqla, M.J. Al-Afghany, A.B. Abo-Hasseira, I.H. Elmasry, A.M. Tabasi, M.D. Alwan, Effect of immersion time of glass powder on mechanical properties of concrete contained glass powder as cement replacement, *Construction and Building Materials*, 206 (2019) 674-682.
- [51] I. Jawed, J. Skalny, Alkalies in cement A review II. Effects of alkalies on hydration and performance of Portland cement, *Cement and Concrete Research*, 8 (1978) 37-52.
- [52] G.C. Edwards, R.L. Angstadt, The effect of some soluble inorganic admixtures on the early hydration of portland cement, *Journal of Applied Chemistry*, 16 (1966) 166-168.
- [53] H.A. Ali, D. Xuan, C.S. Poon, Assessment of long-term reactivity of initially lowly-reactive solid wastes as supplementary cementitious materials (SCMs), *Construction and Building Materials*, 232 (2020) 117192.
- [54] R. Kondo, M. Daimon, E. Sakai, H. Ushiyama, Influence of inorganic salts on the hydration of tricalcium silicate, *Journal of Applied Chemistry Biotechnology*, 27 (1977) 191-197.
- [55] Y. Sun, C.S. Poon, Effect of seawater on the hydration of tricalcium silicate, In: Kovler K., Zhutovsky S., Spatari S., Jensen O. (eds) *Concrete Durability and Service Life Planning. ConcreteLife 2020. RILEM Bookseries*, vol 26. Springer, Cham, (2020).
- [56] A. Kumar, G. Sant, C. Patapy, C. Gianocca, K.L. Scrivener, The influence of sodium and potassium hydroxide on alite hydration: Experiments and simulations, *Cement and Concrete Research*, 42 (2012) 1513-1523.
- [57] M. Etxeberria, A. Gonzalez-Corominas, P. Pardo, Influence of seawater and blast furnace cement employment on recycled aggregate concretes' properties, *Construction and Building Materials*, 115 (2016) 496-505.
- [58] C. Hu, Z. Li, A review on the mechanical properties of cement-based materials measured by nanoindentation, *Construction and Building Materials*, 90 (2015) 80-90.
- [59] P.D. Tennis, H.M. Jennings, A model for two types of calcium silicate hydrate in the microstructure of Portland cement pastes, *Cement and Concrete Research*, 30 (2000) 855-863.
- [60] Z. Luo, W. Li, Y. Gan, K. Mendu, S.P. Shah, Applying grid nanoindentation and maximum likelihood estimation for N-A-S-H gel in geopolymers paste: Investigation and discussion, *Cement and Concrete Research*, 135 (2020) 106112.
- [61] G. Constantinides, F.-J. Ulm, The effect of two types of C-S-H on the elasticity of cement-based materials: Results from nanoindentation and micromechanical modeling, *Cement and Concrete Research*, 34 (2004) 67-80.
- [62] E. Bernard, B. Lothenbach, F. Le Goff, I. Pochard, A. Dauzères, Effect of magnesium on calcium silicate hydrate (C-S-H), *Cement and Concrete Research*, 97 (2017) 61-72.

- [63] C. Roosz, P. Vieillard, P. Blanc, S. Gaboreau, H. Gailhanou, D. Braithwaite, V. Montouillout, R. Denoyel, P. Henocq, B. Madé, Thermodynamic properties of C-S-H, C-A-S-H and M-S-H phases: Results from direct measurements and predictive modelling, *Applied Geochemistry*, 92 (2018) 140-156.
- [64] B. Mota, T. Matschei, K. Scrivener, Impact of NaOH and Na₂SO₄ on the kinetics and microstructural development of white cement hydration, *Cement and Concrete Research*, 108 (2018) 172-185.
- [65] M.J. Sánchez-Herrero, A. Fernández-Jiménez, Á. Palomo, L. Klein, Alkaline hydration Of C₂S and C₃S, *Journal of the American Ceramic Society*, 99 (2016) 604-611.
- [66] B. Mota, T. Matschei, K. Scrivener, The influence of sodium salts and gypsum on alite hydration, *Cement and Concrete Research*, 75 (2015) 53-65.
- [67] J.W. Bullard, H.M. Jennings, R.A. Livingston, A. Nonat, G.W. Scherer, J.S. Schweitzer, K.L. Scrivener, J.J. Thomas, Mechanisms of cement hydration, *Cement and Concrete Research*, 41 (2011) 1208-1223.
- [68] A. Traetteberg, P.E. Grattan - Bellew, Hydration of 3CaO • Al₂O₃ and 3CaO • Al₂O₃+gypsum with and without CaCl₂, *Journal of the American Ceramic Society*, 58 (1975) 221-227.
- [69] A.K. Suryavanshi, J.D. Scantlebury, S.B. Lyon, Mechanism of Friedel's salt formation in cements rich in tri-calcium aluminate, *Cement and Concrete Research*, 26 (1996) 717-727.
- [70] H. Hirao, K. Yamada, H. Takahashi, H. Zibara, Chloride binding of cement estimated by binding isotherms of hydrates, *Journal of Advanced Concrete Technology*, 3 (2005) 77-84.
- [71] N. Hadded, M. Bouanz, Electrical conductivity of the binary mixture isobutyric acid–water with added (Zn²⁺, SO₄²⁻) ions, *Fluid Phase Equilibria*, 266 (2008) 47-53.
- [72] S.-T. Lee, D.-W. Park, K.-Y. Ann, Mitigating effect of chloride ions on sulfate attack of cement mortars with or without silica fume, *Canadian Journal of Civil Engineering*, 35 (2008) 1210-1220.
- [73] O. Al-Amoudi, Rasheeduzzafar, M. Maslehuddin, S. Abduljawwad, Influence of chloride ions on sulphate deterioration in plain and blended cements, *Magazine of Concrete Research*, 46 (1994) 113-123.
- [74] C. Qiao, P. Suraneni, J. Weiss, Damage in cement pastes exposed to NaCl solutions, *Construction and Building Materials*, 171 (2018) 120-127.
- [75] T. Kim, I.-T. Kim, K.-Y. Seo, H.-J. Park, Strength and pore characteristics of OPC-slag cement paste mixed with polyaluminum chloride, *Construction and Building Materials*, 223 (2019) 616-628.
- [76] X. Wang, W. Ni, R. Jin, B. Liu, Formation of Friedel's salt using steel slag and potash mine brine water, *Construction and Building Materials*, 220 (2019) 119-127.
- [77] M. Zajac, J. Skocek, P. Durdzinski, F. Bullerjahn, J. Skibsted, M. Ben Haha, Effect of carbonated cement paste on composite cement hydration and performance, *Cement and Concrete Research*, 134 (2020) 106090.
- [78] B.J. Zhan, D.X. Xuan, C.S. Poon, C.J. Shi, Mechanism for rapid hardening of cement pastes under coupled CO₂-water curing regime, *Cement and Concrete Composites*, 97 (2019) 78-88.
- [79] E.T. Stepkowska, J. Pérez-Rodríguez, M. Sayagues, J. Martínez-Blanes, Calcite, vaterite and aragonite forming on cement hydration from liquid and gaseous phase, *Journal of Thermal Analysis and Calorimetry*, 73 (2003) 247-269.
- [80] E.T. Stepkowska, Simultaneous IR/TG study of calcium carbonate in two aged cement pastes, *Journal of Thermal Analysis and Calorimetry*, 84 (2006) 175-180.
- [81] S. Goto, K. Suenaga, T. Kado, M. Fukuhara, Calcium silicate carbonation products, *Journal of the American Ceramic Society*, 78 (1995) 2867-2872.
- [82] J. Bukowski, R.L. Berger, Reactivity and strength development of CO₂ activated non-hydraulic calcium silicates, *Cement and Concrete Research*, 9 (1979) 57-68.

- [83] J.I. Bhatti, Hydration versus strength in a portland cement developed from domestic mineral wastes—A comparative study, *Thermochimica Acta*, 106 (1986) 93-103.
- [84] E. Berodier, K. Scrivener, Evolution of pore structure in blended systems, *Cement and Concrete Research*, 73 (2015) 25-35.
- [85] P. Lawrence, M. Cyr, E. Ringot, Mineral admixtures in mortars, *Cement and Concrete Research*, 33 (2003) 1939-1947.